UNIVERSITY OF OKLAHOMA GRADUATE COLLEGE

Utilizing Auxetic Materials in Responsive Facades for Optimal Daylighting in the Office Building

A THESIS

SUBMITTED TO THE GRADUATE FACULTY

in partial fulfillment of the requirements for the

Degree of

Master of Science

By Shiva Azizi
Norman, Oklahoma

2025

Utilizing Auxetic Materials in Responsive Facades for Optimal Daylighting in the Office Building

A THESIS APPROVED FOR THE

CHRISTOPHER C. GIBBS COLLEGE OF ARCHITECTURE

BY THE COMMITTEE CONSISTING OF

Dr. Negar Heidari Matin, Chair
Dr. Shideh Shadravan
Dr. Shakil Shimul

Abstract:

The purpose of this thesis is to explore the integration of auxetic materials into responsive façades for optimizing daylighting and visual comfort in office buildings. By using their negative Poisson's ratio (NPR), auxetic structures passively adapt to solar exposure by expanding perpendicularly to applied forces, enabling dynamic shading without mechanical systems.

Through parametric modeling, 36 façade configurations were generated and structurally validated using Karamba3D. Climate-based simulations (Honeybee/Ladybug) evaluated performance using three metrics: Useful Daylight Illuminance (UDI): % of time illuminance stays within 300–3000 lux (optimal range), Spatial Daylight Autonomy (sDA): % of floor area receiving ≥300 lux for ≥50% of occupied hours, and Daylight Glare Probability (DGP): % of time glare remains <0.45 (acceptable comfort). The 4×6 panel configuration at 90° actuation (Scenario 24) achieved the best balance: 79% UDI (daylight availability), 61.36% sDA (spatial coverage), and 93.71% glare comfort (6.6% improvement over the unshaded baseline).

These results validate auxetic façades as a passive, energy-efficient solution that simultaneously enhances daylight sufficiency (meeting LEED standards) and visual comfort, advancing sustainable building envelope design.

Keywords: Auxetic materials, Responsive facades, Daylighting optimization, Parametric design

Table of Contents

LIST OF FIGURES.. 2
LIST OF TABLES.. 3
LIST OF EQUATIONS.. 6
ABSTRACT 7
CHAPTER 1: INTRODUCTION..8
1.1 Background and Context 8
1.2 Auxetic Materials and Their Unique Behavior 8
1.3 Daylighting and Glare 9
1.3.1 Useful Daylight Illuminance (UDI) 10
1.3.2 Spatial Daylight Autonomy (sDA) 10
1.3.3 Daylight Glare Probability (DGP) 11
1.4 Responsive Façade 11
1.5 Parametric Design 11
1.6 Problem Statement 12
1.7 Research Questions 12
1.8 Research Objectives 13
1.9 Significance of Study 13
1.10 Limitations 14
1.11 Structure of the Thesis 14
CHAPTER 2: LITERATURE REVIEW 15
2.1 Auxetic Materials..15
2.2 Auxetic MaterialsProperties..18
2.3 Applications of Auxetic Materials in Other Disciplines..20
CHAPTER 3: RESEARCH METHODOLOGY 21
CHAPTER 4: RESULTS AND DISCUSSION..23
4.1 Auxetic Panel Configurations..23
4.2 Structural Validation of Auxetic Behavior Using Karamba3D..28
4.3 Daylight Simulation Results..30
4.3.1 Evaluation of (UDI) and(sDA)..33
4.3.2 Evaluation of Daylight Glare Probability (DGP)..40
CHAPTER 5: CONCLUSION AND RECOMMENDATIONS..53
CHAPTER 6: REFERENCES..54

List of Figures

Figure 1.1 Responses of materials under tensile stress, differentiated by Poisson's ratios: positive, zero, and negative — Author's illustration……………………………………….…**7**

Figure 2.1 Mechanical properties of auxetic materials, including energy absorption, enhanced strength, and programmable reconfigurability — Author's illustration………………………...**18**

Figure 3.1 Research workflow for the design, structural analysis, and daylight performance evaluation of auxetic façades — Author's illustration…………………………….…………**20**

Figure 4.1 Matrix of 36 auxetic façade design scenarios across three panel sizes (4×6, 6×10, 12×18) and six actuator angles — Author's parametric model outputs…………………………**24**

Figure 4.2 Comparison of two auxetic panel designs illustrating responsive behavior through inner auxetic deformation and outer SMP activation — Author's parametric simulation outputs……………………………………………………………………………………**26**

Figure 4.3 Structural simulation output showing auxetic behavior under axial strain (Poisson's ratio ≈ –1.15) — Author's Karamba3D analysis…………………………………………...**27**

Figure 4.4 Structural simulation result of second auxetic configuration (Poisson's ratio ≈ –1.09) — Author's Karamba3D analysis…………………………………………..……..**28**

Figure 4.5 Monthly daylight distribution comparison under three shading scenarios: compressed, stretched, and no shading — Author's simulation results in Honeybee……..…….**30**

Figure 4.6 UDI analysis for 12×18 auxetic configurations — Author's Honeybee simulation output…………………………………………………………………….……………………**36**

Figure 4.7 sDA results for 12×18 auxetic configurations — Author's Honeybee simulation output……………………………………………………………………………………….**37**

Figure 4.8 Legend for glare visualization indicating % of time DGP exceeds 0.45 — Author's Honeybee simulation output…………………………………………………………….……**39**

List of Tables

Table 1.1 UDI performance classification ……………………………………………15

Table 1.2 sDA classification based on LEED thresholds ……………………………16

Table 1.3 DGP-based classification of visual comfort levels ………………………17

Table 4.1 Matrix of the 36 auxetic façade design scenarios……………………… 24

Table 4.2 Key performance characteristics of the SMP layer ………………………25

Table 4.3 Mechanical properties assigned to auxetic material ………………………27

Table 4.4 Simulation result: Poisson's ratio ≈ –1.15 ………………………………27

Table 4.5 Simulation result: Poisson's ratio ≈ –1.09 ………………………………28

Table 4.6 Key parameters for daylight simulation ……………………………………29

Table 4.7 Radiance ambient parameters used for daylight simulation ………………30

Table 4.8 Monthly daylight distribution under different shading states ……………30

Table 4.9 UDI, sDA, and LEED results for 6×10 panels ………………………………32

Table 4.10 UDI, sDA, and LEED results for 4×6 panels ………………………………34

Table 4.11 UDI, sDA, and LEED results for 12×18 panels ……………………………36

Table 4.12 DGP results for 6×10 panels ………………………………………………38

Table 4.13 DGP results for 4×6 panels ………………………………………………39

Table 4.14 DGP results for 12×18 panels ……………………………………………40

Table 4.15 Baseline façade performance (no shading) ………………………………41

Table 4.16 Performance metrics of optimal scenario (Scenario 24) …………………42

List of Equations

Equation 1.1 Useful Daylight Illuminance formula……………………………………………….9

Equation 2.1 Definition of Poisson's Ratio………………………………………………………14

Equation 2.2 Hooke's Law — force-displacement relationship……………………………..15

Equation 2.3 Relationships between Young's modulus (E), shear modulus (G), bulk modulus (K), and Poisson's ratio (ν)………………………………………………………………..……15

Equation 2.4 Definition of Young's Modulus — stress–strain relationship………….……..16

Equation 2.5 Shear modulus based on applied force and displacement……………………..…16

Equation 2.6 Bulk modulus as the ratio of pressure change to volume change………..……17

1. Introduction

1.1 Background and Context

There is an ongoing climate crisis that poses a significant challenge to human health and the environment, emphasizing the importance of reducing global carbon dioxide (CO2) emissions as soon as possible. Buildings are contributing significantly to this problem, with approximately 27% of global CO2 emissions resulting from using operational energy to maintain indoor comfort. Moreover, 11% of emissions are attributed to the production of construction materials. Approximately 37% of all emissions are attributed to the built environment [1].

Facades play a crucial role in ensuring occupant comfort and reducing energy consumption. The use of adaptive facades has demonstrated significant potential for reducing the use of active heating and cooling systems. As these facades respond to external conditions, such as sunlight and temperature, they can optimize the indoor climate control. By modifying their orientation, geometry, or thermal properties, adaptive shading systems can increase building energy efficiency and minimize their environmental footprint [2].

1.2 Auxetic Materials and Their Unique Behavior

Auxetic materials, characterized by their **Negative Poisson's Ratio (NPR)**, have garnered significant attention due to their unconventional mechanical behavior and advancements in fabrication technologies [3]. Unlike conventional materials, which contract laterally when stretched, auxetic materials expand perpendicular to the applied force. This unique behavior, first reported by Lakes in 1987, has opened new avenues for innovative applications across various fields. However, the complexity of fabricating auxetic geometries initially limited their practical use [4]. Recent advancements in additive manufacturing (AM) have addressed these challenges, enabling precise and scalable production of auxetic materials. Techniques such as fused filament fabrication (FFF) and laser powder bed fusion facilitate the creation of polymeric and metallic auxetic structures with tailored properties [5]. **Figure 1.1** demonstrates the variation in material behavior under tensile stress according to their Poisson's ratios.

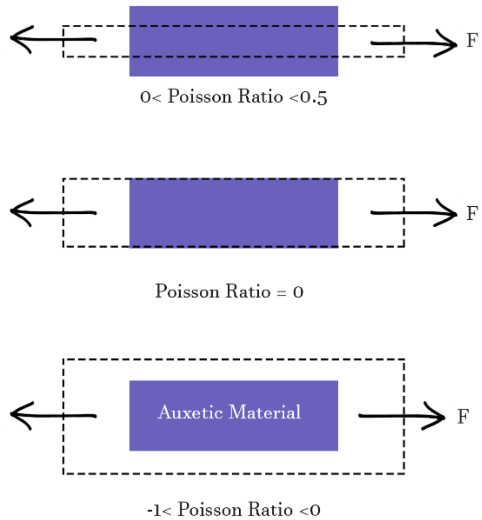

Figure 1.1. Responses of materials under tensile stress, differentiated by Poisson's ratios: positive, zero, and negative — Source: Author's illustration

Numerous industries have used auxetic materials, including apparel [6], automotive [7], aerospace [8], pharmaceuticals [9], sports [10], military [11], biomedical systems [12], and engineering [13]. This unusual behavior is rare in natural materials but can sometimes be observed. More commonly, auxetic properties are engineered through the design of Metamaterials [14] specifically crafted to exhibit properties not typically found in nature that are highly desirable for application in different fields due to their distinctive mechanical characteristics [15]. The properties of auxetic material could include the ability to absorb more energy [16], resist indentation [17], withstand high shear forces [18], resist impacts and fractures [19], enhance acoustic damping [20], conduct heat, and electricity efficiently [21], and adjust permeability based on the load applied [22] allowing them to dynamically respond to varying mechanical forces, which is particularly advantageous in applications like adaptive filtration, fluid management, and pressure-sensitive devices [23].

1.3. Daylighting and Glare

Window openings play a crucial role in inviting daylight into interior spaces, serving not only to connect the indoor and outdoor environments and enhance human health and well-being, but also to harness daylight as a valuable energy resource, reducing reliance on artificial lighting. In this context, employees work approximately 2,000 hours each year, with beneficial daylight being accessible for more than 75% of those hours, underscoring the effectiveness of well-designed openings in optimizing natural light utilization. In modern office buildings, the desire for clear and attractive facades often results in a high proportion of windows to walls [24]. This allows more solar radiation to enter, increasing the need for air conditioning to keep the interior comfortable [25]. Architectural shading can help block this radiation, but if not designed properly, it can also reduce daylight access and outside views [26]. Finding the right balance between allowing daylight, preserving views, and reducing energy use is a key challenge. Additionally, while integrating daylight into indoor environments has been shown to enhance user satisfaction and support energy efficiency, improperly controlled daylight can result in excessive brightness. This often leads to glare and visual discomfort, negatively affecting focus and visual comfort [27]. According to recent studies, optimizing these elements can substantially improve occupant satisfaction and productivity [28].

Dynamic daylight metrics—such as spatial Daylight Autonomy (sDA), and Useful Daylight Illuminance (UDI) are particularly effective for assessing indoor daylight distribution, glare potential, and daylight-responsive lighting controls.

1.3.1. Useful Daylight Illuminance (UDI)

Useful Daylight Illuminance (UDI) quantifies daylight availability as the percentage of annual occupied hours when illuminance levels remain within the optimal 300-3000 lux range at a given point. Following IESNA standards [29], a space is considered adequately daylit when it achieves ≥300 lux for at least 50% of occupied hours. In this study, UDI is calculated as:

$$\mathrm{UDI} = \left(\frac{\text{Hours with } 300 \leq \text{Illuminance} \leq 3000 \text{ lux}}{\text{Total occupied hours}} \right) \times 100$$

Equation 1.1. Useful Daylight Illuminance formula

UDI (% of time)	Daylight Performance Level	Interpretation
<50%	Poor	Space fails to meet minimum daylight requirements for most occupied hours
50-70%	Moderate	Space meets basic daylight autonomy but may need supplemental lighting
70-85%	Good	Well-daylit space with minimal glare risk
>85%	Excellent	Optimal daylight availability with potential glare control needed

Table 1.1. UDI performance classification based on the percentage of occupied hours within 300–3000 lux range [29]

1.3.2. Spatial Daylight Autonomy (Sda)

Spatial Daylight Autonomy (sDA) defines what amount of a space collects enough daylight. Precisely, it defines the percentage of floor zone that obtains no less than 350 lux for at least 50% of the yearly inhabited hours. The rate of sDA results varies from 0 to 100%. While spatial Daylight Autonomy (sDA) effectively predicts daylight distribution and uniformity, it does not evaluate visual glare.

sDA	Status
0-50%	LEED failed
50-75 %	Accepted
More than 75%	Preferred

Table 1.2. sDA classification based on LEED daylighting credit thresholds

1.3.3. Daylight Glare Probability (DGP)

To address this limitation, Daylight Glare Probability (DGP) evaluates visual comfort by analyzing luminance distributions within space. The metric calculates glare risk on a scale from 0 to 1, where lower values indicate better comfort. This study measures DGP as the percentage of annual occupied hours below the 0.45 threshold, with classifications adapted from [30]:

DGP Range	Visual Comfort Level	Interpretation
DGP < 0.35	High Comfort	Glare is imperceptible
0.35 ≤ DGP < 0.40	Moderate Comfort	Glare is perceptible but not disturbing
0.40 ≤ DGP < 0.45	Acceptable Comfort	Glare may be noticeable but remains tolerable
DGP > 0.45 in > 5% of occupied time	Discomfort Glare	Visual discomfort is likely; mitigation recommended

Table 1.3. DGP-based classification of visual comfort levels, adapted from [30]

Higher percentages of time spent in lower DGP ranges (<0.45) indicate superior visual comfort. The metric is derived from high dynamic range (HDR) imaging of luminance distributions in the field of view.

1.4. Responsive Façade

An innovative architectural approach to enhancing both energy efficiency and occupant comfort is responsive facades, a design concept that adapts to environmental conditions. A variety of mechanisms are used in these systems to respond to factors such as sunlight, temperature, and the needs of occupants, thus maximizing the performance of the building. Responsive facades often incorporate kinetic elements, such as hexagonal modules or origami-inspired designs, which adjust to sunlight exposure, reducing solar heat gain and glare [31].

1.5. Parametric Design

To analyze and predict the performance of responsive facades, computational models are often employed early in the design process to facilitate informed decision-making. These models enable designers to assess and refine their approaches, enhancing the functionality and efficiency of the facades. [32]. One of these computational software is Grasshopper. Grasshopper is a plug-in for Rhinoceros that shows the users with a visual interface language to make and modify geometry. Grasshopper is based on nodes, components and graphs put on canvas to make the map that flows relations from parameters to user-defined functions. Each change on parameter will change other parameters.

Honeybee and Ladybug are simulation tools integrated with the Grasshopper plugin for Rhinoceros, designed to enhance building performance through environmental analysis. Honeybee facilitates detailed energy and daylight simulations, aiding in optimizing a building's energy efficiency. Ladybug, conversely, allows for the analysis and visualization of weather data, providing insights into climatic conditions to inform sustainable design decisions. Together, these tools are instrumental in enabling architects to create buildings that are both energy-efficient and harmoniously attuned to their environments [33].

1.6. Problem Statement

One of the most challenging aspects of integrating daylight as a primary source of lighting in office buildings is managing glare while maintaining an adequate level of daylight and external views. A traditional fixed shading system may not adapt to the changing sun position throughout the day and across seasons, resulting in excess glare or reduced daylight and obstructed views. This trade-off limits the effectiveness of daylight strategies and negatively impacts the comfort and productivity of occupants.

While responsive facades offer greater flexibility due to their dynamic adjustment to solar conditions, most current systems rely on conventional materials and mechanisms that may not respond efficiently or seamlessly. The unique properties of auxetic materials allow them to be used to create facade geometries that are adaptable to climate conditions, allowing daylight to be managed and glare to be minimized without compromising visibility.

Although auxetic materials have been extensively studied in fields such as engineering and biomedical applications, their potential for integration into architectural systems, particularly for daylight optimization in adaptive facades, remains largely underexplored. This study seeks to bridge this gap by leveraging the unique mechanical properties of auxetic to design responsive facade systems, with a focus on enhancing indoor environmental quality.

1.7. Research Questions

-What are the optimal design parameters (e.g., Cell Size, Number of Cells, Actuators Angel) for achieving the desired Negative Poisson’s Ratio (NPR) and improving daylight performance metrics such as UDI, DGP, and sDA?

-Can auxetic materials be effectively integrated into responsive facade systems to optimize daylighting and energy efficiency in office buildings?

-Which actuation mechanisms are most suitable for deforming auxetic structures in response to sunlight exposure, and how can they be integrated into facade systems?

1.4. Research Objectives

-Explore Applications of Auxetic Materials in Other Disciplines
Conduct a comprehensive review of the properties and applications of auxetic materials in fields such as **medical science**, **aerospace**, and **sports engineering**. Emphasize their unique mechanical characteristics and functional advantages in these disciplines to identify transferable principles relevant to architectural systems.

-Adapt Non-Architectural Strategies for Facade Design
Analyze design methodologies, material configurations, and functional uses of auxetic materials in non-architectural applications, such as biomedical devices (e.g., stents, implants). Extract and reinterpret these strategies to inform the development of adaptive, high-performance facade systems.

-Develop Parametric Models for Responsive Facade Systems
Employ advanced parametric modeling tools, including **Rhino** and **Grasshopper**, to design facades incorporating auxetic geometries. Investigate design parameters such as cell size, cell number, and actuator angles to optimize both **daylighting performance** and **structural efficiency**.

-Assess Feasibility of Auxetic Facades
Validate the mechanical and structural behavior of the proposed auxetic facade systems using simulation platforms named **Karamba3D**. Simultaneously, evaluate their daylighting performance through comprehensive **annual daylight simulations** using tools like **Ladybug** and **Honeybee** to ensure their practical applicability and effectiveness in real-world contexts.

-Propose Innovative Facade Solutions for Energy Efficiency
Develop cutting-edge responsive facade systems that dynamically adjust to environmental conditions, particularly sunlight exposure. Optimize these designs for **enhanced daylight penetration** and **glare control**, contributing to sustainable and human-centric architectural practices.

1.8. Significance of Study

This research pioneers the use of auxetic materials in architectural applications, addressing environmental challenges and advancing daylighting strategies. It proposes energy-efficient facade systems that reduce reliance on artificial lighting, improve occupant comfort, and contribute to sustainable building practices. Leveraging interdisciplinary insights and parametric design tools, this study offers a practical framework for integrating auxetic materials into responsive architectural systems.

1.9. Limitations

Although this research aims to provide a thorough understanding of how auxetic materials can enhance building facades, there are a few limitations to keep in mind:

1. Material Availability: Auxetic materials are not widely available and may be expensive, which could limit how feasible it is to implement these designs on a larger scale.
2. Simulation-Based Results: The study relies on computer simulations to model and test the designs. While these tools are highly advanced, they may not perfectly represent how the facades would perform in real-life scenarios. Physical prototypes and testing are not included in this study.
3. Specific Climatic Context: The findings of this study are primarily focused on office buildings in Norman, Oklahoma, which may limit external validity when applied to different climatic regions or building types. Future research should explore the adaptability of auxetic facades in other environmental and architectural contexts.
4. Design Constraints: The study assumes ideal conditions for auxetic materials and does not address challenges like manufacturing or construction hurdles that might arise in practice.

1.10. Structure of the thesis

This thesis is organized into five chapters that guide the reader through the research process, from the initial context to the final findings and conclusions.

Chapter 1: Introduction
Provides an overview of the climate crisis and the role of buildings in energy consumption, followed by a discussion on daylighting, glare, responsive facades, and auxetic materials. The chapter concludes with the problem statement and outlines the significance and scope of the research.

Chapter 2: Literature Review
Examines existing research related to auxetic materials, their mechanical behavior, and applications in architecture. It also explores studies on daylighting performance, glare control, and responsive facade systems. This chapter identifies knowledge gaps and establishes the theoretical foundation for the study.

Chapter 3: Methodology
Describes the research approach, including parametric modeling using Rhino and Grasshopper, structural analysis with Karamba3D, and daylight simulation with Honeybee and Ladybug. It

details how auxetic geometries are integrated into responsive facade systems and outlines the criteria for performance evaluation.

Chapter 4: Results and Discussion
Presents the outcomes of the simulations and analysis, focusing on daylight metrics such as UDI, sDA, and DGP. The results are discussed in relation to facade design variables, such as cell size and actuator rotation, with insights into how auxetic behavior influences daylight performance and visual comfort.

Chapter 5: Conclusion and Recommendations
Summarizes the key findings of the study, reflects on the research contributions, and offers recommendations for future applications of auxetic materials in architectural facades. Suggestions for further research are also included.

2. Literature Review

In recent years, advancements in materials engineering have driven significant interest in adapting innovative materials to improve building performance, addressing challenges related to energy efficiency, sustainability, and occupant comfort

2.1. Auxetic Materials

In recent years, advancements in materials engineering have driven significant interest in adapting innovative materials to improve building performance, addressing challenges related to energy efficiency, sustainability, and occupant comfort [34].
One such breakthrough is the development and application of auxetic materials, which exhibit extraordinary mechanical properties compared to conventional materials. When a material is stretched, it typically becomes longer in the direction of the stretch and narrower across it. This behavior is described by Poisson's ratio (μ), a measure of how much a material shrinks or expands sideways when stretched or compressed. Most materials have a positive Poisson's ratio, meaning they get thinner when stretched and thicker when compressed. Auxetic materials, however, exhibit the opposite behavior—they expand sideways when stretched and become narrower when compressed, making them fundamentally different from conventional materials [35]. Poisson's ratio (ν) is defined as the negative ratio of transverse strain to axial strain:

$$\nu = -\frac{\varepsilon_{\text{transverse}}}{\varepsilon_{\text{axial}}}$$

Equation 2.1: Definition of Poisson's Ratio

Where:

- **εaxial** is the strain in the direction of applied load

- **εtransverse** is the strain perpendicular to the load direction.

For most conventional materials, Poisson's ratio is positive, meaning they become thinner in the transverse direction when stretched. For example, for metals and polymers, $-0.25 < \nu < 0.3$. Glasses and minerals are more compressible, and for these $\nu \rightarrow 0$. For gases and cork, $\nu = 0$. For auxetic materials, $\nu < 0$. This negative value of Poisson's ratio signifies that the material or structure exhibits auxetic properties, meaning they expand laterally when stretched and contract laterally when compressed [36].
The mechanical properties of auxetic materials, characterized by their negative Poisson's ratio, enhance their performance in a wide range of applications. Their properties improve their performance in various applications. To fully understand these enhanced mechanical behaviors, it is essential to explore the theoretical framework that governs material deformation, particularly the principles of elasticity derived from **Hooke's Law**. This foundation provides insight into how auxetic materials respond uniquely to applied stress compared to conventional materials.

Hooke's Law is fundamental in describing the elastic behavior of materials when subjected to external forces. It states that the force F required to extend or compress a material is proportional to displacement X, and is expressed mathematically as:

$$F = kX$$

Equation 2.2: Hooke's Law — force-displacement relationship

Where:

-F is the applied force,

-X is the resulting displacement,

-k is the stiffness constant (specific to the material).

This relationship applies to ideal linear elastic materials and serves as the basis for defining other important mechanical properties such as **Young's modulus (E)**, **Shear modulus (G)** and **Bulk modulus (K)**. These constants help quantify a material's resistance to various types of deformation.

For isotropic materials, the following relationships hold:

$$G = \frac{E}{2(1+\nu)} \quad \text{and} \quad K = \frac{E}{3(1-2\nu)}$$

Equation 2.3: Relationships between Young's modulus E, shear modulus G, bulk modulus K, and Poisson's ratio ν

Where:

-ν is Poisson's ratio,

-E is Young's modulus,

-G is shear modulus,

-K is bulk modulus.

These formulas demonstrate how changes in Poisson's ratio—particularly when negative in auxetic materials—significantly influence a material's shear and volumetric response, thereby contributing to their enhanced mechanical performance.

Also referred to as the tensile modulus or elastic modulus, **Young's modulus** measures a material's stiffness under uniaxial stress. It is defined as:

$$E = \frac{\sigma}{\varepsilon}$$

Equation 2.4: Definition of Young's Modulus — stress–strain relationship

Where:

-σ is tensile stress (force per unit area)‘

-ε is tensile strain (relative deformation).

This modulus describes how resistant a material is to being stretched or compressed, with higher values indicating greater stiffness. The SI unit is Pascal (Pa).

The shear modulus quantifies a material's response to shear stress—forces acting parallel to its surface. It is calculated using the formula:

Where:

$$G = \frac{F \cdot l}{A \cdot \Delta x}$$

Equation 2.5: Shear modulus based on applied force and displacement in a material

-F is the applied tangential force,

-l is the initial length,

-A is the area over which the force is applied,

-Δx is the transverse displacement.

The shear modulus reflects how a material deforms under twisting or shearing forces.

The bulk modulus measures a material's resistance to uniform compression. It is expressed as:

Where:

$$K = -V\left(\frac{\Delta P}{\Delta V}\right)$$

Equation 2.6: Bulk modulus as the ratio of pressure change to volume change

-V is the original volume,

-ΔP is the change in pressure,

-ΔV is the change in volume.

A high bulk modulus indicates that a material is less compressible, which is especially relevant in structures exposed to high-pressure environments. These theoretical relationships help explain the origin of the exceptional mechanical behaviors observed in auxetic materials. With a clearer understanding of the underlying elastic principles, we can now examine the key mechanical properties that make auxetic materials valuable across various industries and scientific applications.

2.2 Auxetic Materials Properties

Auxetic materials have a high specific energy absorption (SEA), so they can efficiently absorb and dissipate energy during high-velocity impacts or sudden forces, such as car crashes or falls. Due to their unique geometry, they deform significantly under stress, [37] making them ideal for automotive crash protection and protective gear applications, which must absorb impact energy to reduce injuries and damage [38]. For instance, an asymmetrical re-entrant triangular honeycomb structure increases specific energy absorption (SEA) by 291% over a traditional honeycomb structure [39]. Furthermore, they enhances a material's Young's modulus, which measures its stiffness and ability to resist deformation under various loads. Due to this enhancement, auxetic materials are precious in sectors requiring high structural integrity and resilience. Optimizing the stiffness-to-weight ratio is vital in aerospace and civil engineering [40]. As a result, auxetic materials and structures perform better under mechanical stress, extending their lifespan and functionality [41]. For example, auxetic carbon fiber composites demonstrate significantly higher buckling strength than non-auxetic composites. Experimental and simulation studies reveal that the critical buckling loads of auxetic composites are approximately three times higher, emphasizing the impact of the negative Poisson's ratio on enhancing yield strength [42]. In addition to these properties, auxetic textiles and polymeric materials exhibit superior shear resistance and fracture toughness [43]. They perform mechanically under stress because of their unique structural configurations, such as chiral and re-entrant geometries [44]. It is also important to highlight that materials with auxetic properties have increased indentation resistance, making them suitable for protective applications. These materials can resist localized pressures or forces without permanently deforming. Because auxetic materials have a negative

Poisson's ratio when subjected to localized stress, surface damage and denting are less likely to occur [45]. They also offer improved vibration-dampening and sound absorption capabilities, which are beneficial in various industrial and consumer settings [46]. Another significant attribute is the High flexural modulus of auxetic materials which measures their resistance to bending [47]. This can prevent them from failing under higher flexural loads [48]. This property is crucial in applications where structural components, such as beams and panels, are subject to bending forces [49]. They have a high strain tolerance, which allows them to withstand significant deformations without breaking. As a result, they are ideal for applications requiring high levels of flexibility and durability [50]. Materials with auxetic properties can also adjust their porosity due to mechanical stress, enabling them to control fluid or gas flow [51]. The ability to dynamically regulate permeability is vital in filtration systems, breathable fabrics, and medical devices where permeability can be controlled dynamically [52]. Acoustic damping is another area where auxetic materials excel, they effectively absorb and dissipate sound energy [53]. Due to their unique structure, they are ideal for noise reduction applications in industries like construction, automotive, and soundproofing [54]. Moreover, auxetic materials with negative thermal expansion contract when heated, unlike most materials that expand. This property is valuable in precision engineering applications, such as aerospace and electronics, where maintaining dimensional stability under varying temperatures is critical [55]. Additionally, they can form synclastic curvatures, meaning they bend into dome-like shapes when stretched [56]. This unique ability makes them ideal for applications requiring curved, load-bearing structures, such as helmets, architectural components, and protective gear [57], and the last one is their programmability and reconfigurability refer to the ability of these materials to dynamically change shape in response to external stimuli, [58] such as temperature, pressure, or mechanical forces [59]. Because of this adaptive ability, auxetic materials are ideal for use in innovative materials, robotics, and wearable technology, where dynamic performance and flexibility are required [60].

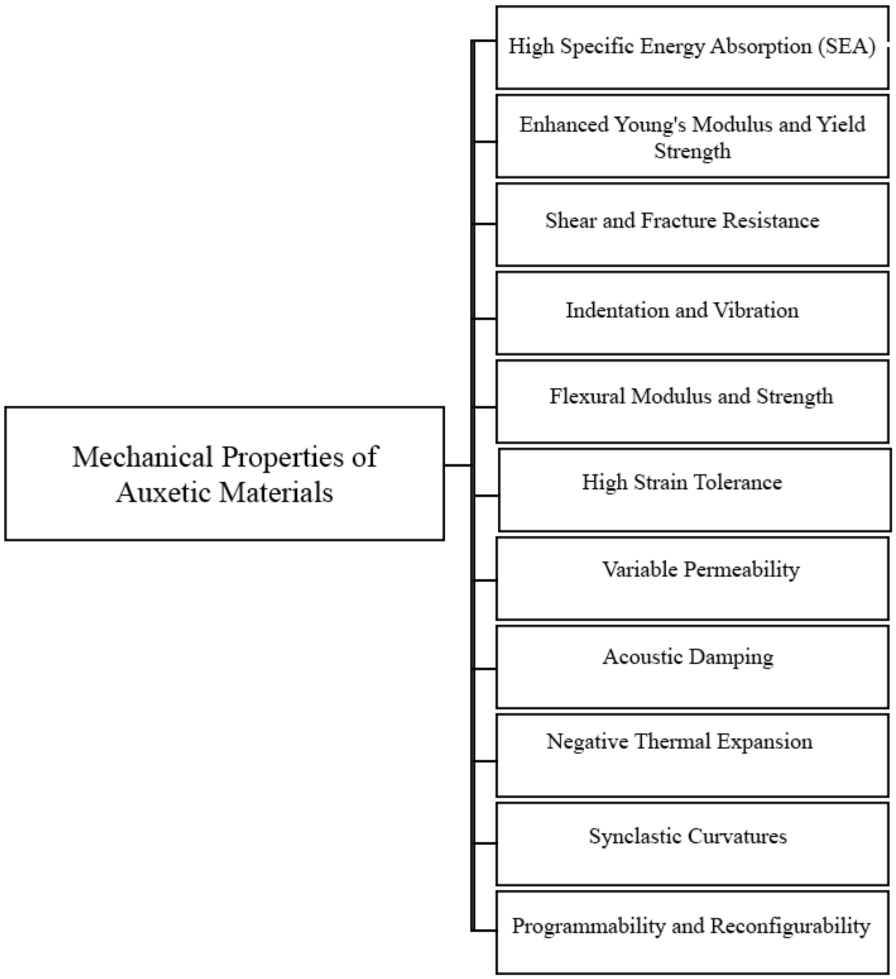

Figure 2.1. Mechanical properties of auxetic materials, including energy absorption, enhanced strength, and programmable reconfigurability. *Source: Author's illustration.*

2.3 Applications of Auxetic Materials in Other Disciplines

While auxetic materials have not yet been widely adopted in architecture, their application across fields such as biomedical engineering [61], sports equipment [62], fashion [63], automotive [64], and aerospace industries [65] demonstrates their remarkable potential for structural and adaptive innovation. For example, in Biomedical they are used for stent [66], Implant [67], wound dressing [68], Scaffold [69], Sensors [70]. These applications demonstrate properties that could be translated into architecture, such as adaptive facades that respond to wind or sunlight, impact-resistant cladding, or ventilated panels that respond to environmental input. Therefore, auxetic materials represent a promising direction for future architectural research, particularly in relation to performance-driven, responsive envelope systems.

The use of auxetic materials in architectural facade systems continues to be largely unexplored, despite their widespread use in fields such as biomedical engineering, sportswear, and aerospace for their exceptional mechanical properties. With auxetic structures' potential to expand laterally under tensile stress, they provide a valuable opportunity for designing passively responsive facades, especially for climate-responsive and occupant-centered buildings.

Currently, not enough research has been conducted on how auxetic geometries can be incorporated into building envelopes to improve daylighting performance, especially when using simulation-based approaches. The majority of current daylighting studies in architecture emphasize mechanically operated or static shading systems without taking into account how auxetic behavior may influence passively light penetration and glare control.

Additionally, there are few studies that provide a unified parametric workflow that integrates the evaluation of structural and environmental performance of auxetic systems.

Given these gaps, this thesis proposes a novel investigation into how auxetic materials can be parametrically modeled, structurally validated, and environmentally optimized for responsive facades in office buildings. The study bridges disciplines by leveraging auxetic mechanical adaptability not only for structural performance but also for enhancing daylight distribution, reducing glare, and supporting visual comfort critical aspects of occupant well-being.

3. Research Methodology

The aim of this thesis is to propose an algorithmic and parametric-based auxetic shading design as a responsive facade strategy for office buildings in Norman. This strategy reduces uncomfortable glare, improves daylight quality, and preserves outward views by physically allowing the facade to respond to sunlight. The approach addresses occupant needs and environmental demands through a material-informed geometric system that deforms in reaction to solar exposure. The overall workflow is illustrated in **Figure 3.1.**, outlining the three main phases of the research process.

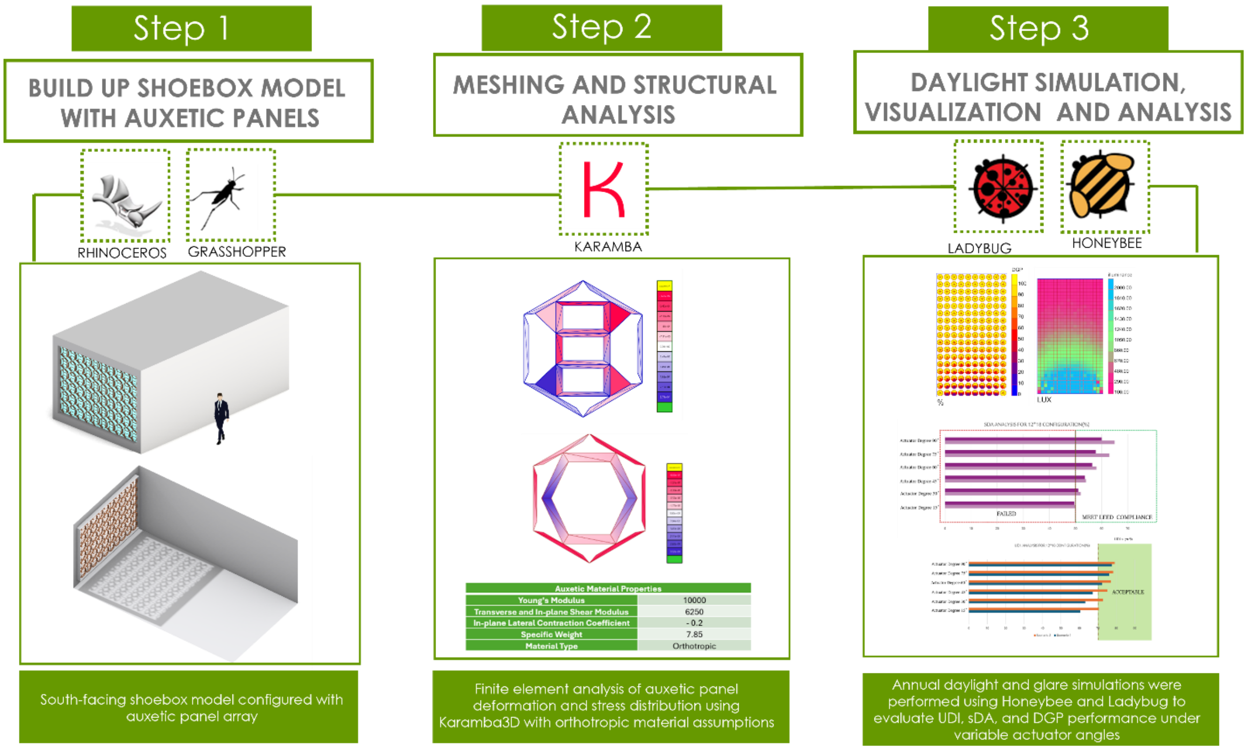

Figure 3.1. Research workflow for the design, structural analysis, and daylight performance evaluation of auxetic façades using Rhinoceros, Grasshopper, Karamba3D, Ladybug, and Honeybee. *Source: Author's illustration.*

Phase 1: Shoebox Model Build-Up

The first phase focuses on developing a simplified office space model to serve as the testing ground for the auxetic shading system. A shoebox-type office is created using Rhinoceros 3D and Grasshopper, with a south-facing facade. The responsive shading system is modeled parametrically using an auxetic pattern applied to the glazing. Design variables such as cell size, unit count, and actuator angles are controlled to simulate geometric responsiveness to solar exposure. Polyurethane-based shape memory polymers (PU-SMPs) are considered as a potential real-world material for implementing the responsive mechanism due to their thermal adaptability and shape recovery characteristics.

Phase 2: Meshing and Structural Analysis

The second phase investigates the structural behavior and auxetic characteristics of the proposed shading system. The parametric geometry is transformed into a mesh and analyzed using Karamba3D, a structural simulation plugin within the Grasshopper environment. The material is modeled as orthotropic with properties suitable for flexible architectural components. Simulations are conducted under axial loading to evaluate deformation patterns. The resulting negative Poisson's ratio confirms the auxetic response of the system, validating its suitability for a responsive facade that can dynamically adapt to environmental stimuli.

Phase 3: Daylight Simulation and Analysis

The third phase of this study evaluates the environmental performance of the responsive auxetic facade through climate-based daylight simulations. The analysis is conducted using the Ladybug and Honeybee plugins in Grasshopper, applying local climate data from Norman, Oklahoma. A simplified office model is used to simulate daylighting conditions for a total of 36 auxetic shading setups, each varying in cell number, size and actuator rotation. The performance of each configuration is assessed using key daylight metrics, including Useful Daylight Illuminance (UDI), Spatial Daylight Autonomy (sDA), and Daylight Glare Probability (DGP). This phase focuses on understanding how responsive auxetic geometry affects daylight penetration and glare control in office spaces, laying the groundwork for analysis in the following chapter.

4.Result and Discussion

This chapter presents and analyzes the results from simulation studies on the performance of auxetic shading systems in office buildings. It focuses on how different configurations of auxetic materials affect daylight distribution, glare control, and the responsiveness of facades under specific climatic conditions. Through parametric modeling and computational analysis, the study assesses the potential of auxetic-based shading to enhance visual comfort, energy efficiency, and architectural adaptability.

4.1. Auxetic Panel Configurations

The following table illustrates various configurations of auxetic panels tested in simulation studies designing in rhino, grasshopper. Each panel configuration is represented at different actuator angels, cell number and cell size demonstrating how the geometry adapts and aligns with environmental factors such as sunlight angle. This visual representation supports the analysis of how each configuration contributes to daylight optimization and glare reduction.

Number of Auxetic panels (x*y)	Visulaization
4*6	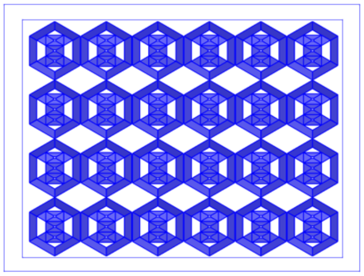 15˚ 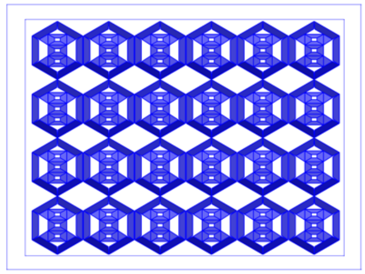 30˚ 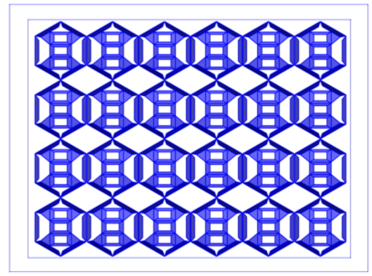 45˚ 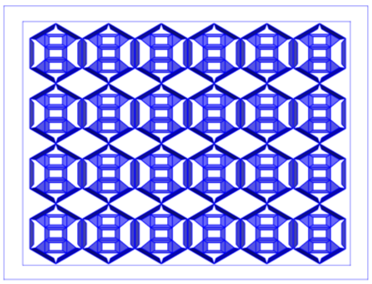 60˚ 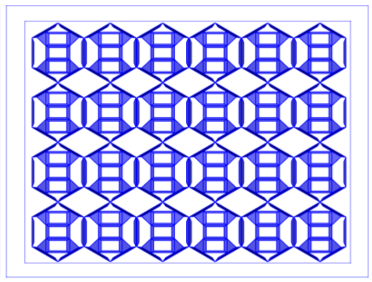 75˚ 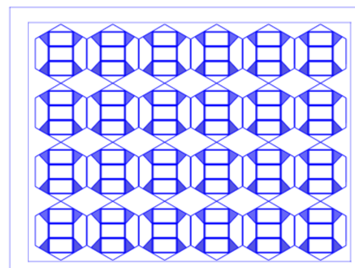 90˚
6*10	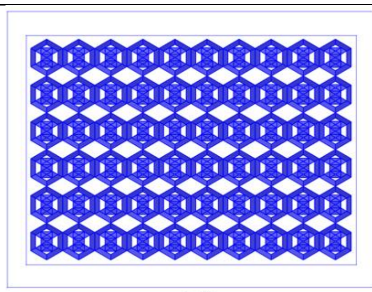 15˚ 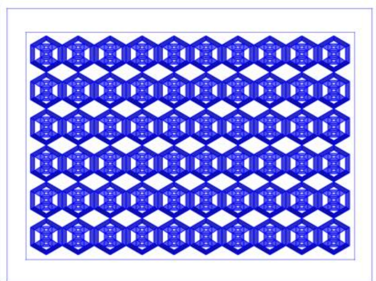 30˚ 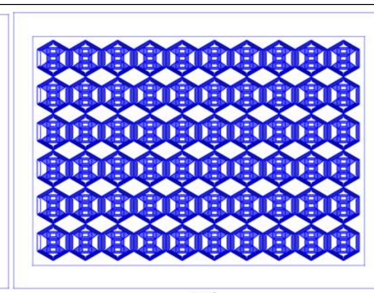 45˚ 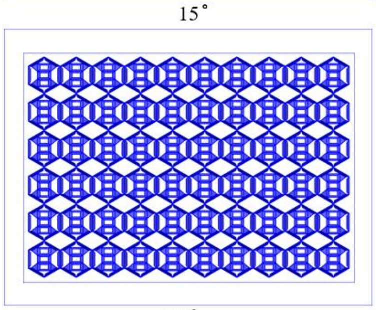 60˚ 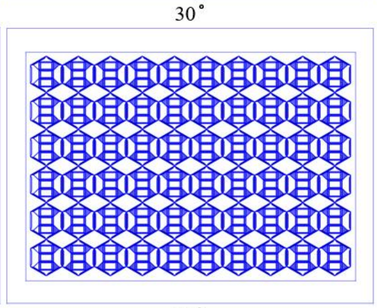 75˚ 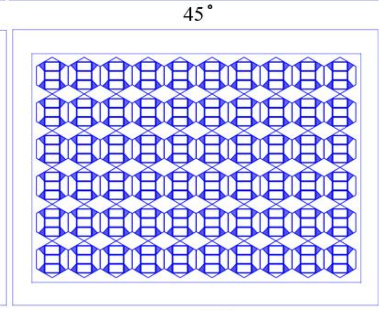 90˚

12*18	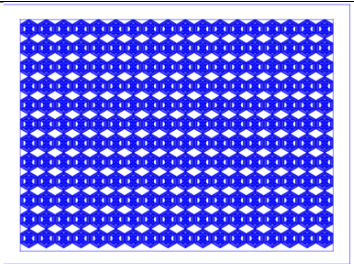 15˚ 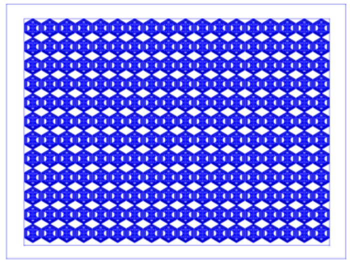 30˚ 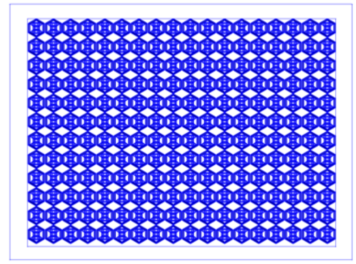 45˚ 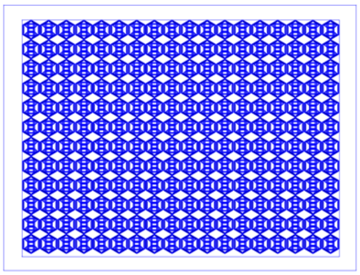 60˚ 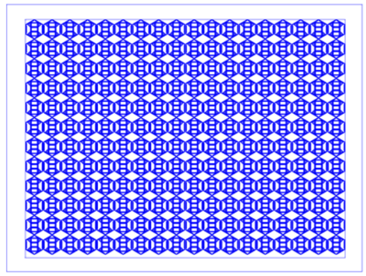 75˚ 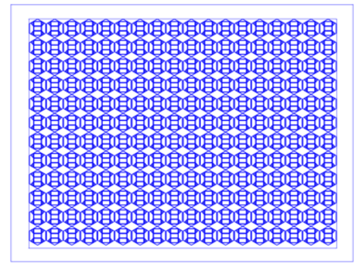 90˚
4*6	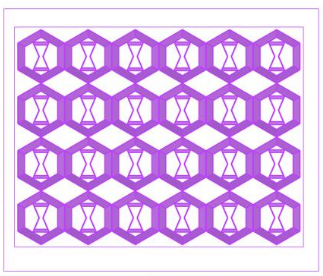 15˚ 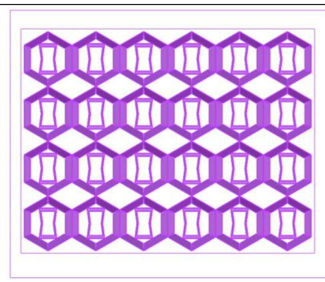 30˚ 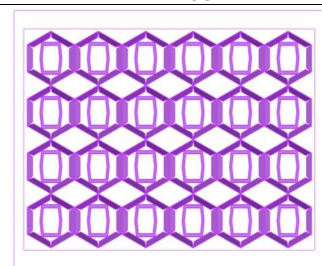 45˚ 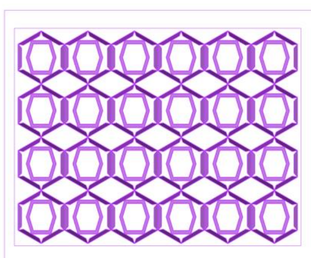 60˚ 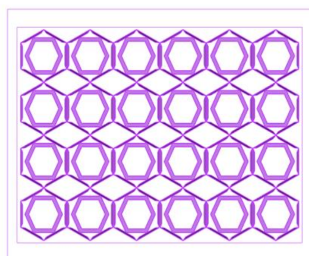 75˚ 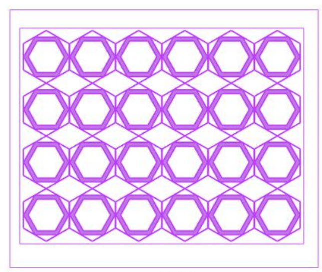 90˚

6*10	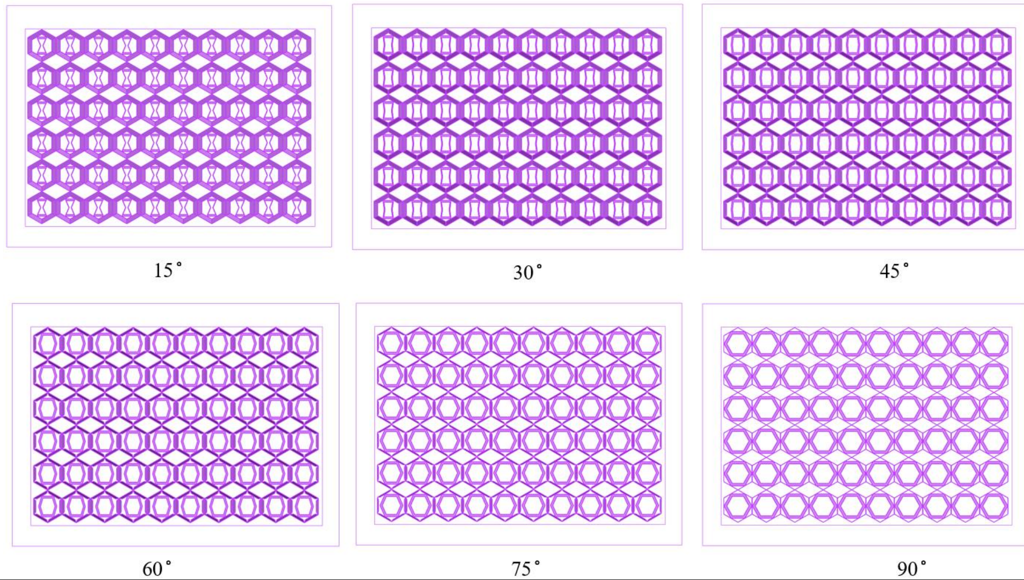
12*18	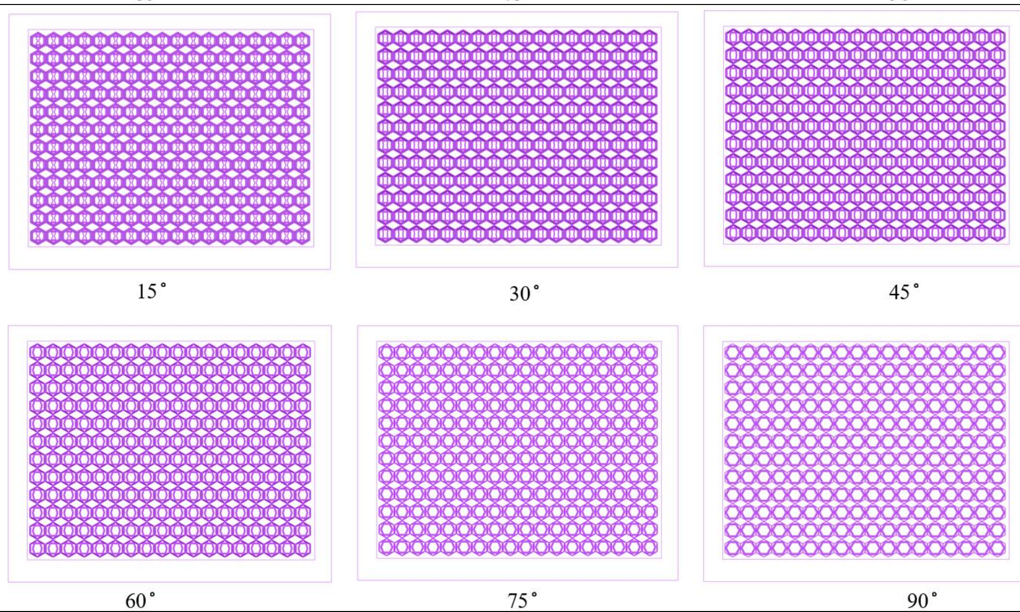

table 4.1. Complete matrix of the 36 auxetic façade design scenarios used in this study, showing two auxetic design types across three panel sizes (4×6, 6×10, 12×18) and six actuator angles (15°, 30°, 45°, 60°, 75°, 90°). These variations were parametrically modeled in Grasshopper and used for both structural and daylight simulation. *Source: Author's parametric model outputs.*

Building on the discussion of auxetic panel configurations, the innovative use of **shape memory polymers (SMPs)** particularly **polyurethane-based SMPs (PU-SMPs)**—significantly enhances the dynamic functionality of facade systems. These materials serve as intrinsic actuators, enabling the facade to autonomously adapt to solar exposure through their thermally responsive shape-memory behavior.

Our panel is composed of two distinct parts: the outer layer, which features the SMPs that react to temperature changes, and the inner layer, designed with a flexible auxetic structure that mechanically responds to the movements of the outer layer.

1. **The outer layer** of each panel, made from polyurethane-based SMPs, actively responds to changes in solar heat. As the temperature increases, these SMPs are triggered, reverting from a temporarily deformed state to their original shape. This transformation is crucial as it drives the mechanical action of the facade system, enabling the panels to rotate and thus adjust their orientation to optimally manage sunlight exposure.

Key characteristics of the SMP layer	
Activation threshold	Tunable Tg to match climatic conditions
Recovery efficiency	>90% strain recovery, ensuring consistent actuation over repeated cycles
Durability	Resistance to UV degradation and thermal fatigue

Table 4.2. Key performance characteristics of the Shape Memory Polymer (SMP) layer used in the responsive façade system. *Source: Author's synthesis from material specifications.*

2. **The inner layer** accompanying the active outer layer, the inner layer of the panels supports and enhances the overall adaptive mechanism. Made from materials that complement the SMPs, such as high-density flexible polymers, this layer maintains structural integrity while facilitating necessary deformations. This dual-layer setup ensures that the facade not only responds dynamically to environmental conditions but also remains durable and effective over time.

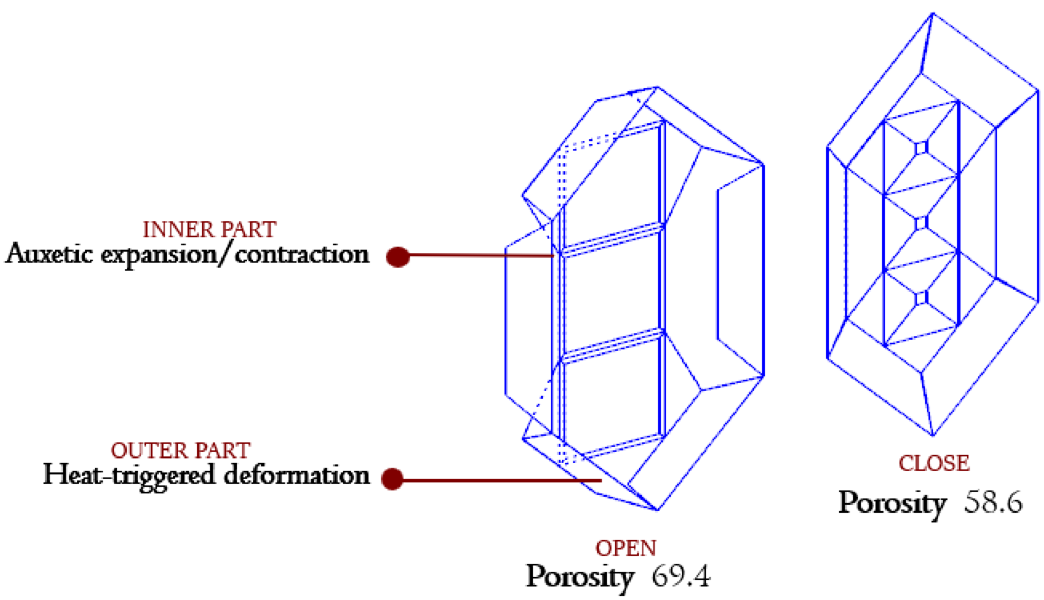

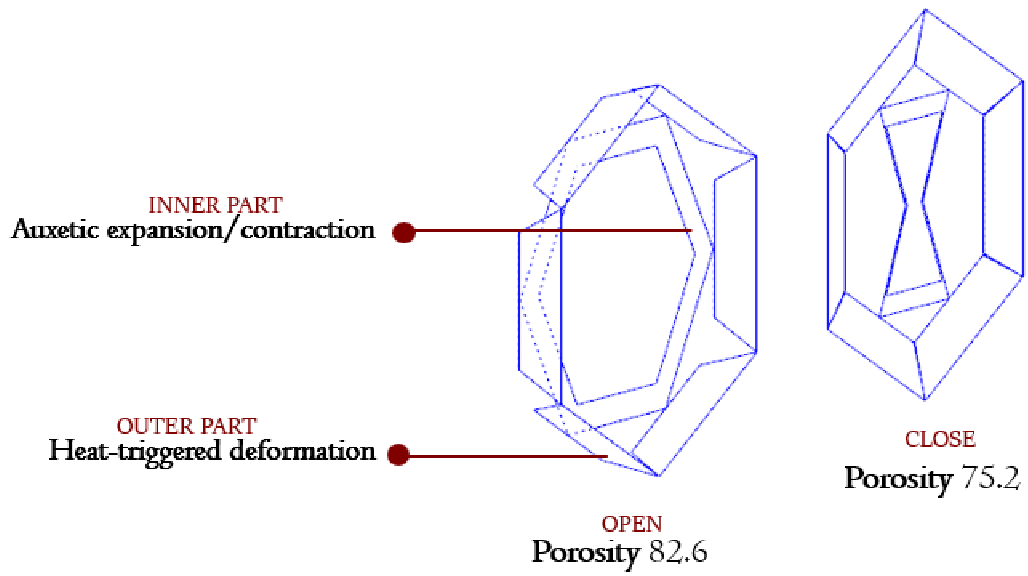

Figure 4.1. Comparison of two auxetic panel designs illustrating responsive behavior through inner auxetic deformation and outer SMP activation. Each panel transitions between open and closed states to adapt to environmental conditions. *Source: Author's parametric simulation outputs.*

4.2. Structural Validation of Auxetic Behavior Using Karamba3D

To validate the auxetic properties of the facade panels, Karamba3D, an advanced parametric structural analysis tool integrated with Grasshopper and Rhino, was employed. This tool allows for a detailed analysis of complex structures under varied loading conditions, making it ideal for assessing the behavior of materials designed with specific mechanical properties. Karamba3D was utilized to simulate the real-world mechanical stresses that facade panels would likely encounter. The panels, composed of an orthotropic material known for its negative Poisson's ratio, were subjected to axial loads. The response measured both axial and transverse strains, which are pivotal in determining the Poisson's ratio and thereby confirming the auxetic nature of the material.

Two key simulations were performed. In the first case, the axial strain was -0.66 and the transverse strain was -0.571579, resulting in a Poisson's ratio of approximately -1.154. In the second case, with an axial strain of -0.34641 and a transverse strain of -0.3775, Poisson's ratio was calculated as -1.09. These negative values confirm that the panels are auxetic, expanding laterally when compressed longitudinally, a unique behavior that can enhance energy absorption and mechanical performance in structural applications.

For a detailed overview of the mechanical properties utilized in these simulations, please refer to the **Auxetic Material Properties Table**. Additionally, the specific results from the simulations are comprehensively presented in the **Simulation Results Table**. These tables provide a clear and structured presentation of both the intrinsic properties of the materials and the empirical data derived from the testing process.

Auxetic Material Properties	
Young's Modulus	10000
Transverse and In-plane Shear Modulus	6250
In-plane Lateral Contraction Coefficient	- 0.2
Specific Weight	7.85
Material Type	Orthotropic

Table 4.3. Mechanical properties assigned to the auxetic material used in structural simulations. Values represent orthotropic behavior, including negative in-plane contraction and defined stiffness parameters for accurate Karamba3D analysis. *Source: Author's simulation input data*

Simulation Result	
Axial Strain type 1	ΔL= -0.66
Transverse Strain type 1	ΔW= -0.571579
Poisson Ratio : ν=- (Axial Strain/Transverse Strain)	**-(-0.571579/0.66) ≈ -1.154**

It is Auxetic!

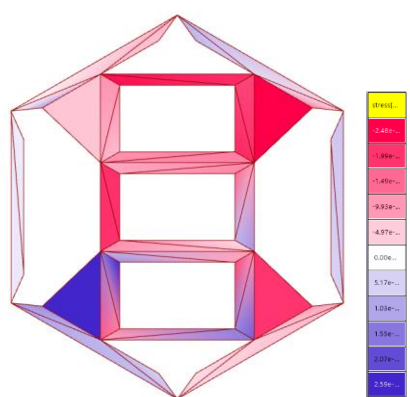

table 4.4. Structural simulation output showing the auxetic behavior of the panel under axial strain. The calculated Poisson's ratio is approximately –1.15, confirming negative lateral expansion and auxetic characteristics. The color gradient visualizes strain distribution across the geometry. *Source: Author's Karamba3D structural analysis.*

Simulation Result	
Axial Strain type 2	ΔL= -0.34641
Transverse Strain type 2	ΔW= -0.3775
Poisson Ratio : ν=- (Axial Strain/Transverse Strain)	**-(-0.3775 /0.34641) ≈ -1.09**
It is Auxetic! 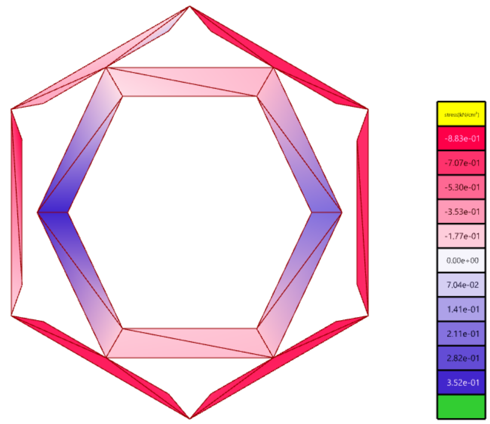	

table 4.5. Simulation result for the second auxetic configuration. The calculated Poisson's ratio of approximately –1.09 confirms the material's auxetic behavior, with visual deformation shown through the strain distribution plot. *Source: Author's Karamba3D analysis.*

4.3. Daylight Simulation Results

Our next step in the evaluation process was to analyze the daylighting performance of the auxetic facade configurations. This involved conducting annual daylight simulations to understand how variations in geometry and actuation influence the amount of natural light entering space and the resulting visual comfort for occupants.

For this purpose, an annual climate-based daylight simulation was conducted to evaluate the performance of various auxetic shading configurations in an office space located in Norman, Oklahoma. A simplified shoebox model measuring 4 meters in width, 9 meters in length, and 3 meters in height was developed to represent a typical office environment. The simulation considered standard working hours from 8:00 AM to 5:00 PM, Monday through Friday. The local climatic conditions were modeled using the Energy Plus Weather (EPW) file for Norman, imported through the Ladybug plugin to ensure accurate environmental input. Daylight performance was assessed using a parametric workflow in Grasshopper, integrating Honeybee and Ladybug to analyze the effectiveness of the facade designs. Key daylighting metrics—including:
Useful Daylight Illuminance (UDI), Measures the percentage of time illuminance falls within the range of 300–3000 lux, indicating comfortable lighting conditions.
Spatial Daylight Autonomy (sDA), Quantifies the percentage of floor area receiving at least 300 lux for 50% of occupied hours. And **Daylight Glare Probability (DGP),** Evaluates the risk

of glare, with values below 0.35 considered acceptable,
were used to determine how each auxetic configuration influenced daylight distribution and visual comfort within space.

Parameters	Values
Space Dimension	4 m (width) × 9 m (length) × 3 m (height)
Location	Norman
Glass	Visible Transmittance = 0.6
Work Plane Height	0.762
Grid Size	0.5
Transmittance of window	0.6

Table 4.6. Key parameters used for daylight simulation, including room dimensions, material properties, and simulation grid settings.*Source: Author's simulation setup in Honeybee.*

Table X presents the Radiance simulation parameters applied in this study to ensure consistent and accurate daylight analysis using the Honeybee plugin in Grasshopper. These settings were uniformly applied across all auxetic facade configurations to maintain a high level of simulation quality. An ambient bounce value of 5 (-ab) was used to capture multiple indirect light reflections, improving the realism of interior daylight distribution. The ambient divisions (-ad) were set to 4096, offering a dense sampling for indirect lighting calculations, while the ambient accuracy (-aa) was kept at 0.1 to balance precision with computational efficiency. Additionally, an ambient resolution of 100 (-ar) was applied to control the spatial detail of the ambient light calculations. These parameters together created a reliable foundation for assessing daylight metrics such as Useful Daylight Illuminance (UDI), Spatial Daylight Autonomy (sDA), and Daylight Glare Probability (DGP) in the responsive facade model.

Ambient bounce (-ab)	**Ambient divisions (-aa)**	**Ambient accuracy (-ad)**	**Ambient Resolution (-ar)**
5	4096	0.1	100

Table 4.7. Radiance ambient parameters used for annual daylight simulation, including bounce, resolution, accuracy, and division values to ensure simulation quality and convergence. *Source: Author's simulation setup in Honeybee.*

Throughout the year, the daylight distribution analysis illustrates the effectiveness of the auxetic facade system under three conditions: compressed (fully closed), stretched (fully open), and without shading panels. When the shading panels are fully compressed, daylight penetration is significantly reduced, resulting in low illuminance levels (under 500 lux) during the summer months, thereby reducing glare and heat gain. The effect of this configuration, however, is to produce under-illumination in transitional months such as March and October. On the other hand, the fully stretched state allows maximum daylight into space, resulting in a more balanced illumination between 300 and 1000 lux, especially during the spring and autumn months. It supports a higher level of daylight autonomy and comfort, although it may lead to slight over-illumination near the facade during the summer months. As a baseline, the no-shading condition exhibits consistently high illuminance levels (often above 2000 lux) throughout the year, particularly from March to October, indicating a high risk of glare and discomfort. Ultimately, the auxetic facade provides a dynamic and efficient method of managing daylight, enhancing comfort, and optimizing energy efficiency throughout the year because of its ability to switch between compressed and stretched states.

Compress Shading Panels

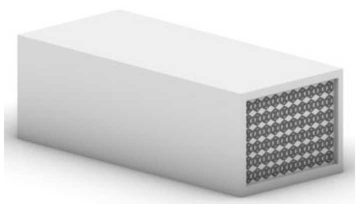

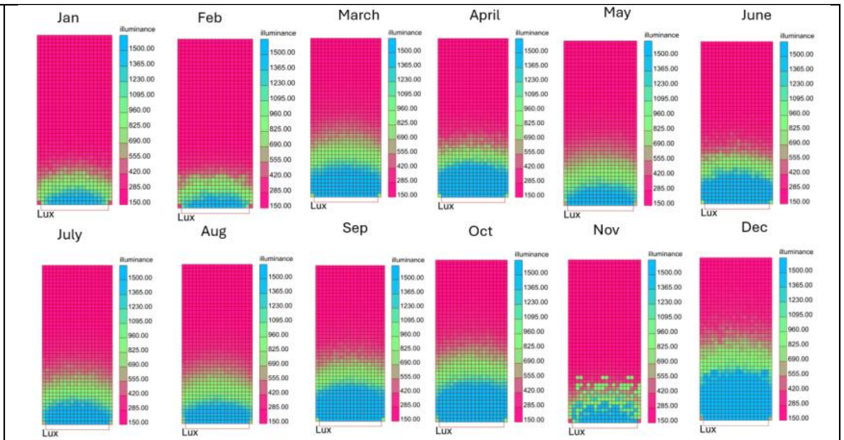

Stretch Shading Panels

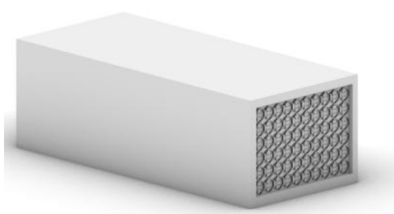

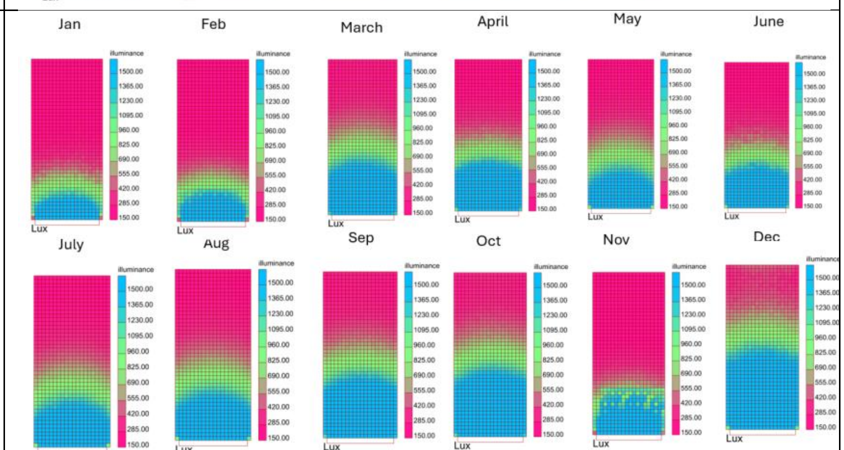

No Shading Panels

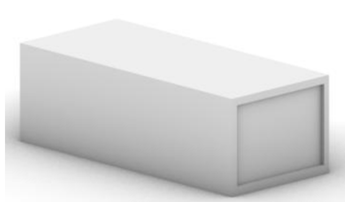

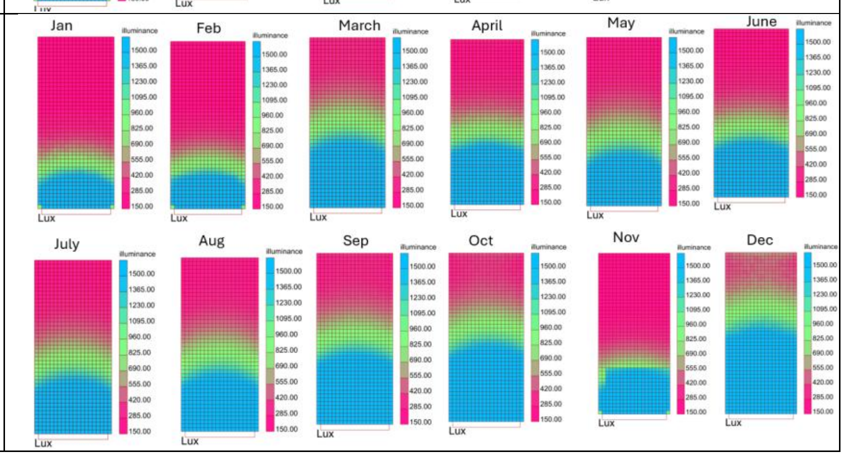

table 4.8. Monthly daylight distribution comparison under three shading scenarios: compressed auxetic panels, stretched auxetic panels, and no shading. The results illustrate the modulation of illuminance levels across the year,

highlighting the effectiveness of responsive auxetic systems in controlling light penetration. *Source: Author's annual simulation results in Honeybee*.

4.3.1. Evaluation of Useful Daylight Illuminance (UDI) and Spatial Daylight Autonomy (sDA)

As a central component of this research, the daylighting performance of two auxetic façade configurations was rigorously evaluated through simulation, using the Useful Daylight Illuminance (UDI) and Spatial Daylight Autonomy (sDA) metrics. These simulations were conducted in Grasshopper with the Honeybee plugin, utilizing Norman, Oklahoma's climate data to ensure accurate environmental responsiveness. The goal was to analyze how varying geometric configurations—specifically, actuator angles and panel densities—affect interior daylight availability and compliance with LEED v4 daylighting standards.

A total of **36 unique scenarios** were developed, representing combinations of three auxetic panel densities (6×10, 4×6, and 12×18) and six actuation angles (15°, 30°, 45°, 60°, 75°, and 90°) across two distinct panel designs. Each design was simulated under consistent environmental and material conditions to isolate the effects of geometry and movement. The results clearly demonstrate a **positive correlation between actuator angle and daylight performance**. For nearly all panel configurations, both UDI and sDA values increased as the actuator angle increased, suggesting that wider geometric openings allow greater daylight penetration into the interior spaces.

Scenarios	Num	Number of Auxetic panels (x*y)	Actuator Degree	UDI %	Sda %	Meet LEED
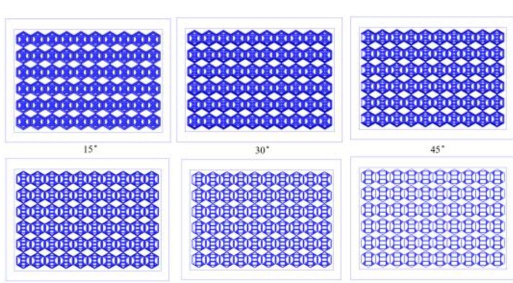	1	6*10	15°	58.50	51	Yes
	2	6*10	30°	59.84	54	Yes
	3	6*10	45°	65.87	55	Yes
	4	6*10	60°	69.85	58	Yes
	5	6*10	75°	74.14	62	Yes
	6	6*10	90°	76.97	67	Yes

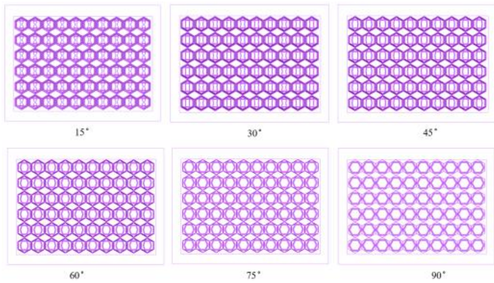	7	6*10	15˚	66.37	45.4	No
	8	6*10	30˚	68.45	46.43	No
	9	6*10	45˚	72.51	49.54	No
	10	6*10	60˚	74.67	52.72	Yes
	11	6*10	75˚	77.20	54	Yes
	12	6*10	90˚	78.25	56.36	Yes

Table 4.9. UDI, sDA, and LEED compliance for 6×10 auxetic panels at different actuator angles. *Source: Author's Honeybee simulations.*

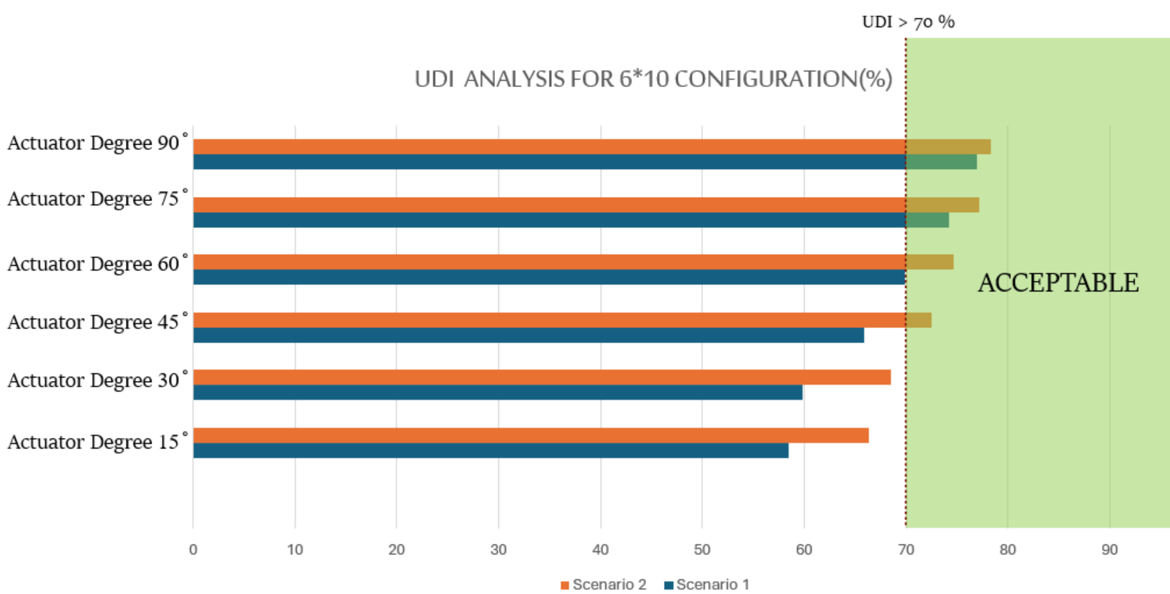

Figure 4.2. UDI performance for the 6×10 auxetic panel configuration across two design scenarios. *Source: Author's Honeybee simulation output.*

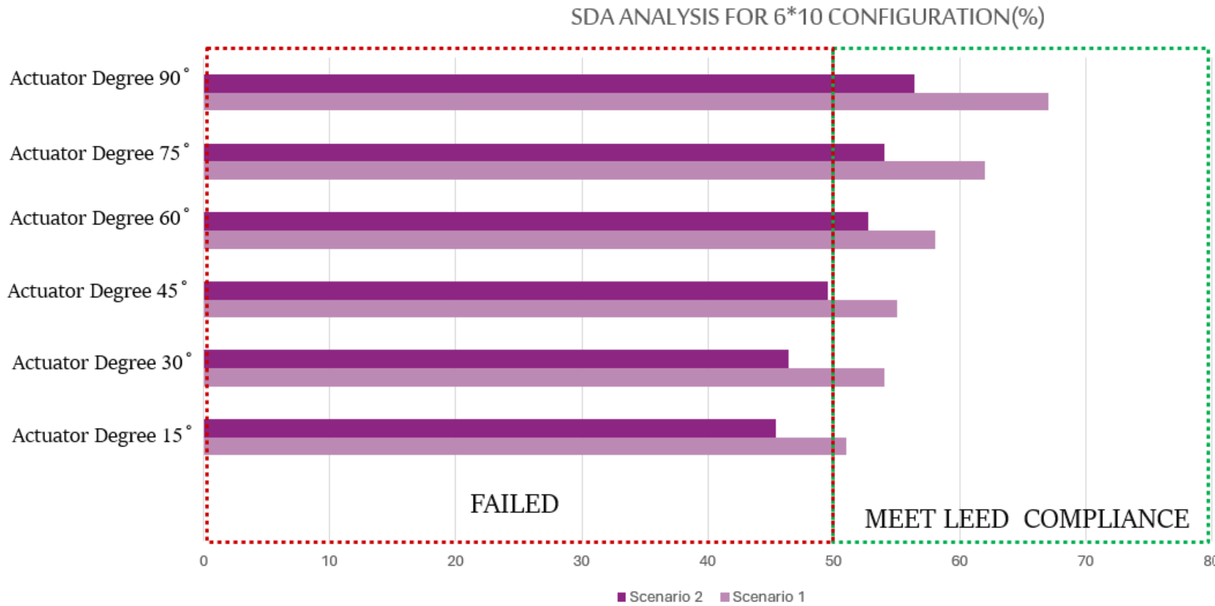

Figure 4.3. sDA analysis for the 6×10 auxetic panel configuration across actuator angles, comparing two design scenarios and their LEED compliance. *Source: Author's Honeybee simulation output.*

In the **6×10 panel configuration**, UDI improved from **58.50% at 15°** to **76.97% at 90°** in the first design, with sDA climbing from **51% to 67%**. The second design showed a similar trend, although some of the lower-angle scenarios did not meet LEED requirements (e.g., sDA = 45.4% at 15°). By 60°, however, both UDI and sDA reached compliant levels, indicating that actuation beyond 45° is critical for effective daylighting in this panel arrangement.

The **4×6 panel configuration**, representing a smaller and more constrained design, showed slightly lower daylight autonomy overall, especially at smaller angles. For example, sDA values in the first design rose from 46% at 15° to 64% at 90°, with compliance beginning at 45°. The second design again outperformed the first in terms of UDI—reaching **79% at 90°**—and maintained LEED compliance from 30° onward. These results suggest that even in smaller façade systems, proper tuning of actuation can yield strong daylight performance when the geometry is optimized.

Scenario	**Num**	**Number of Auxetic panels (x*y)**	**Actuator Degree**	**UDI %**	**Sda %**	**Meet LEED**
	13	4*6	15˚	59.23	46	**No**

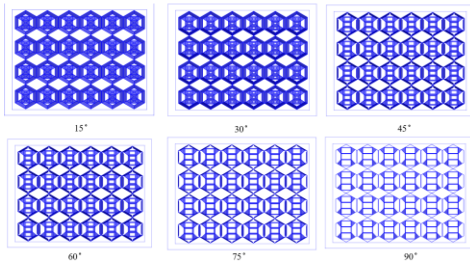	14	4*6	30˚	61.46	49	No
	15	4*6	45˚	65.36	52	Yes
	16	4*6	60˚	71.41	56	Yes
	17	4*6	75˚	75.60	59	Yes
	18	4*6	90˚	77.18	64	Yes
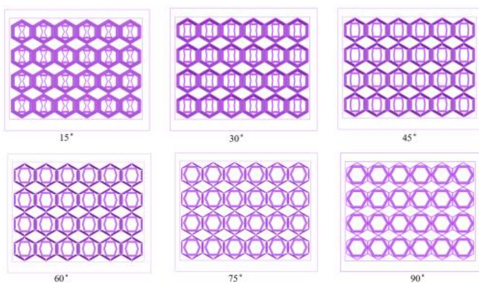	19	4*6	15˚	70.52	48.63	No
	20	4*6	30˚	72.55	50	Yes
	21	4*6	45˚	74.66	53.18	Yes
	22	4*6	60˚	76.81	55.90	Yes
	23	4*6	75˚	78.17	58.63	Yes
	24	4*6	90˚	79	61.36	Yes

Table 4.10. UDI, sDA, and LEED compliance results for 4×6 auxetic panel designs across actuator angles. *Source: Author's Honeybee simulations.*

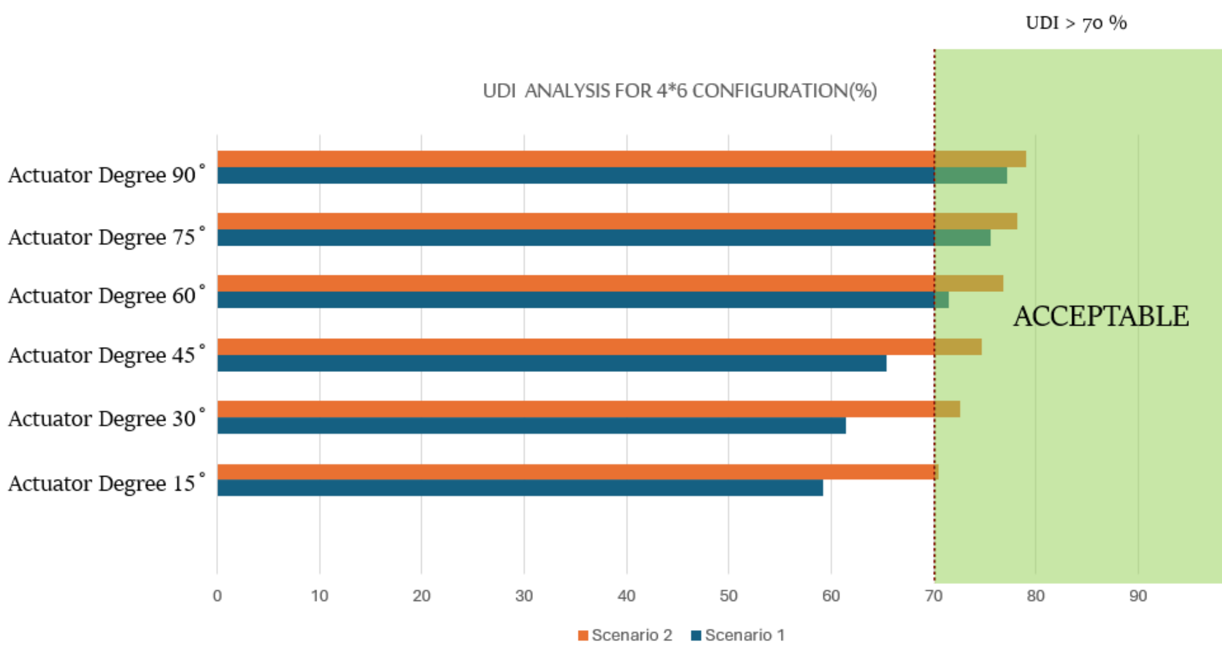

Figure 4.4. UDI results for 4×6 auxetic panel configuration across actuator angles for both design scenarios. *Source: Author's simulation results in Honeybee.*

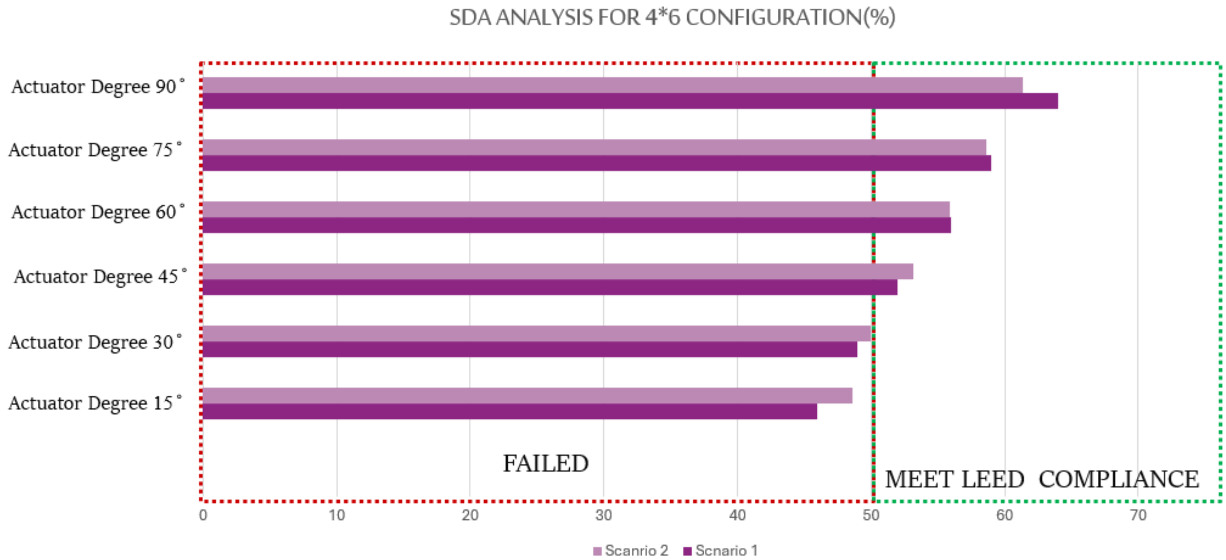

Figure 4.5. sDA analysis for 4×6 auxetic panels across actuator angles, highlighting LEED compliance thresholds. *Source: Author's Honeybee simulation data.*

The **4×6 panel configuration**, representing a smaller and more constrained design, showed slightly lower daylight autonomy overall, especially at smaller angles. For example, sDA values in the first design rose from 46% to 64% at 90°, with compliance beginning at 45°. The second design again outperformed the first in terms of UDI—reaching **79% at 90°**—and maintained LEED compliance from 30° onward. These results suggest that even in smaller façade systems, the proper tuning of actuation can yield strong daylight performance

Scenario	**Num**	**Number of Auxetic panels (x*y)**	**Actuator Degree**	**UDI %**	**Sda %**	**Meet LEED**
	25	12*18	15˚	60.47	50	Yes
	26	12*18	30˚	63.13	52	Yes
	27	12*18	45˚	67.29	54	Yes

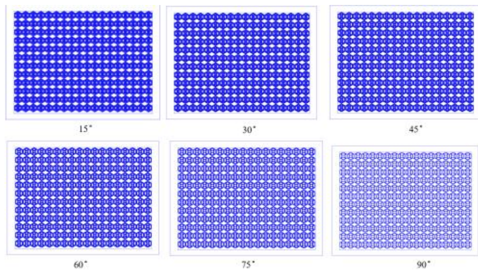	28	12*18	60˚	72.22	58	Yes
	29	12*18	75˚	76.12	63	Yes
	30	12*18	90˚	77.71	65	Yes
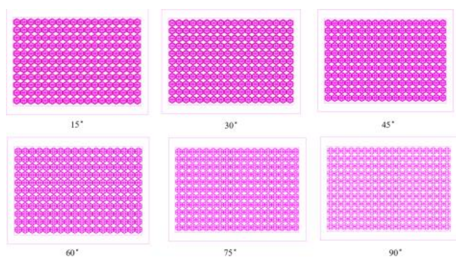	31	12*18	15˚	70.62	49.54	No
	32	12*18	30˚	72.65	51	Yes
	33	12*18	45˚	75.2	53.63	Yes
	34	12*18	60˚	76.98	56.36	Yes
	35	12*18	75˚	78.3	57.72	Yes
	36	12*18	90˚	79.15	60	Yes

Table 4.11. Daylight performance results for 12×18 auxetic panels at various actuator angles. All scenarios meet LEED criteria for sDA. *Source: Author's Honeybee simulation outputs.*

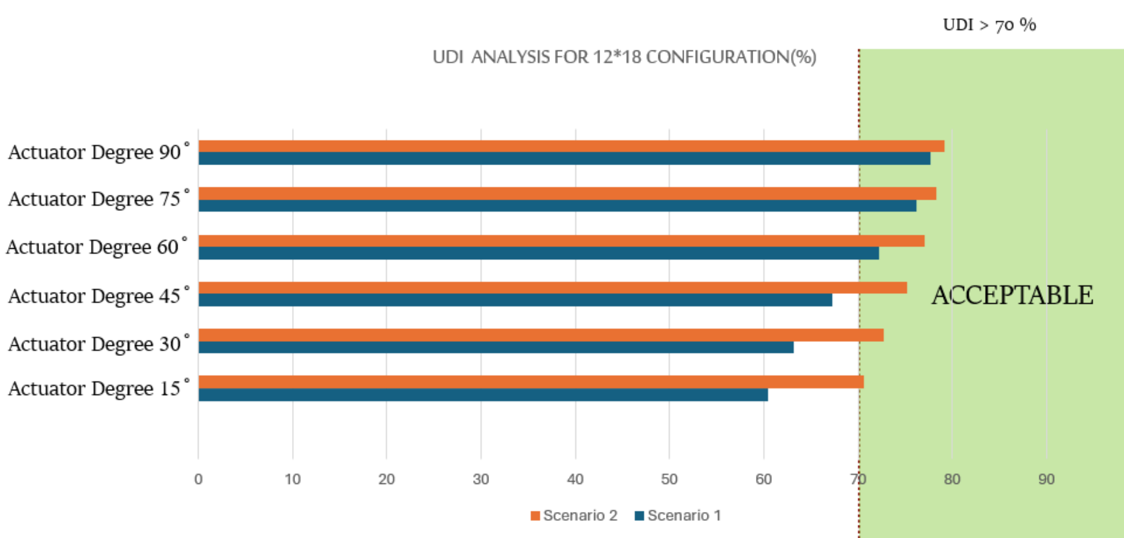

Figure 4.6. UDI analysis for 12×18 auxetic configurations. All actuator angles achieved UDI > 70%, indicating acceptable daylight conditions. *Source: Author's simulation in Honeybee*

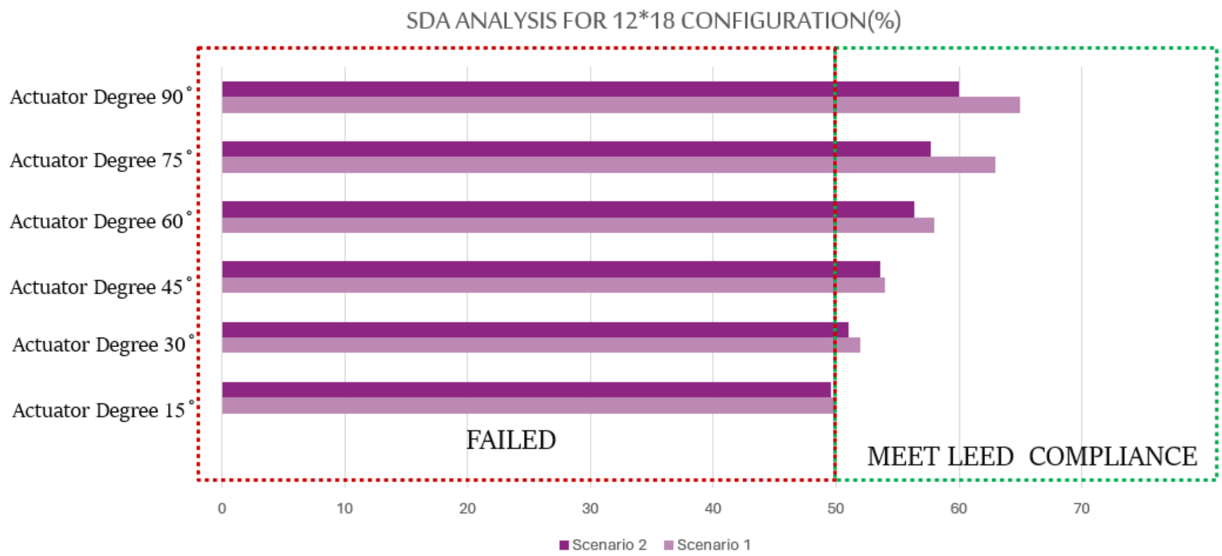

Figure 4.7. sDA results for 12×18 auxetic configurations. Most actuator angles achieved >50% sDA, meeting LEED daylight compliance. *Source: Author's simulation in Honeybee.*

The **12×18 panel configuration**, due to its larger area and higher number of openings, performed the best among all three densities. In both designs, UDI exceeded 60% even at the lowest actuation angles and reached a maximum of **79.15%** at 90° in the second design. sDA also remained consistently strong, ranging from 50% at 15° to 65% at 90°, with most scenarios surpassing LEED thresholds. The performance stability in this configuration demonstrates the advantage of high-density auxetic arrays for achieving uniform and sufficient daylight coverage.

Overall, the **actuator angle proved to be the most influential parameter**, with nearly all configurations achieving LEED daylight compliance at **60° and above**. The **panel density** also played a major role in shaping performance: higher densities provided more control over light diffusion and greater spatial autonomy. Additionally, differences between the two auxetic designs became more evident at higher angles, with the second design generally achieving slightly better UDI values, especially in the 4×6 and 12×18 cases.

This phase of the analysis offers valuable insights into the relationship between geometry, movement, and daylight performance. However, while UDI and sDA address the **quantity and spatial distribution** of daylight, they do not capture **visual comfort** or the potential for glare—factors that are equally important in the design of habitable workspaces. The next phase of the study will therefore focus on **Daylight Glare Probability (DGP)** to complete the evaluation and identify the most balanced and effective façade configuration.

4.3.2. Evaluation of DGP for assessing the visual comfort

Following the daylight sufficiency analysis using UDI and sDA metrics, a detailed evaluation of visual comfort was conducted using Daylight Glare Probability (DGP). This metric provides critical insight into whether occupants are likely to experience discomfort glare due to natural daylight. While UDI and sDA assess how much and where daylight is available, DGP complements these by evaluating the quality of that daylight from a human perspective.

DGP simulations were conducted using the Honeybee plugin in Grasshopper, which incorporates Radiance-based annual glare analysis. Rather than reporting glare as isolated point values, the simulations assessed visual comfort over time at key interior viewpoints. The output is expressed as the percentage of time occupied during hours when the DGP remains below 0.45, the threshold commonly used to define acceptable visual conditions. This metric enables clear interpretation. Higher percentages indicate better visual comfort, as they represent a longer duration during which the space remains free from disturbing or intolerable glare.
The comfort thresholds used in this study follow standard DGP classification [71].

Each of the 36 scenarios (across three auxetic panel sizes and two design types) was evaluated under these criteria to determine which configurations maintain optimal comfort levels throughout the year. To further support the interpretation of Daylight Glare Probability (DGP) results, Honeybee simulations were visualized using a color-coded percentage scale, illustrating the proportion of interior space exceeding the discomfort glare threshold (DGP > 0.45). This spatial representation provides a clearer understanding of how glare is distributed across the occupied area as illustrated in Figure 5.15. In this visualization system:

-0% (represented in yellow) indicates that no part of the space exceeded the DGP threshold, meaning the entire interior remained within comfort limits.

-100% (represented in blue) indicates that the entire space exceeded the threshold, signifying universal discomfort glare.
Intermediate shades (from yellow to blue) represent varying degrees of glare exposure across the space, where increasing blue indicates worsening conditions and reduced comfort.

These visual maps offer immediate insight into the effectiveness of each shading configuration. In early scenarios without shading, large portions of the interior, especially those near glazing areas, were marked in blue—indicating high glare exposure. This confirmed the susceptibility of the space to discomfort glare in the absence of responsive control strategies.

In contrast, scenarios incorporating dynamic auxetic shading systems, particularly those with higher actuator angles (60°, 75°, and 90°), showed maps dominated by yellow or light shades. These results reflect high levels of visual comfort, with DGP remaining below 0.45 across nearly the entire monitored area. This shift from blue to yellow across the simulation sequence demonstrates the effectiveness of auxetic shading in reducing glare and maintaining consistent comfort under variable daylight conditions.

By visualizing glare performance in this manner, the study not only confirms the numerical DGP results but also enhances the spatial understanding of glare control — validating the auxetic system's ability to improve interior visual quality through geometric adaptation.

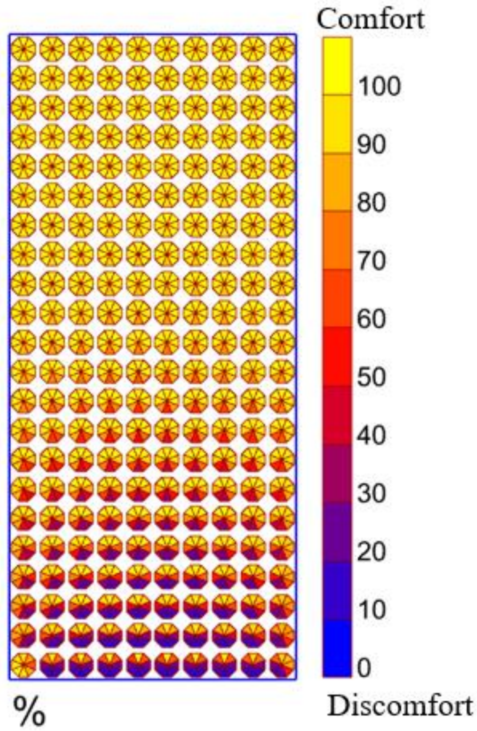

Figure 4.8. Legend for glare visualization indicates the percentage of time DGP exceeds 0.45. Color gradients range from **yellow (comfort)** to **dark blue (discomfort)**. *Source: Author's simulation output from Honeybee.*

Scenarios	Num	Number of Auxetic panels (x*y)	Actuator Degree	% Time DGP < 0.45	Visualization
	1	6*10	15˚	95.49	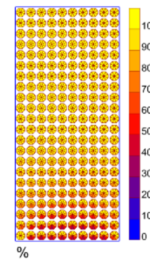
	2	6*10	30˚	95.16	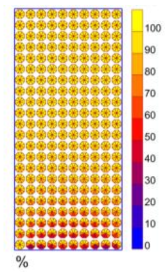
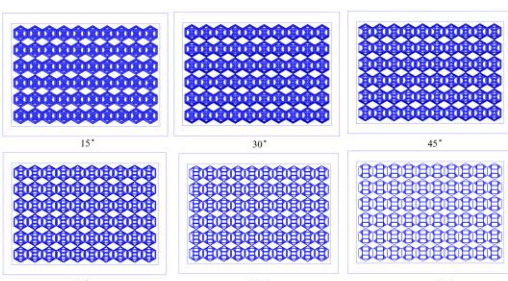	3	6*10	45˚	94.68	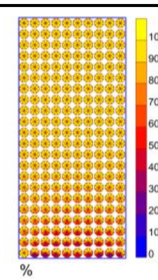
	4	6*10	60˚	93.98	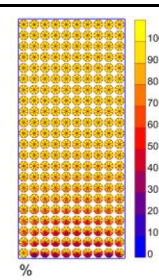

	5	6*10	75˚	93.04	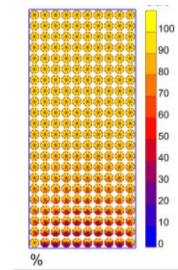
	6	6*10	90˚	91.81	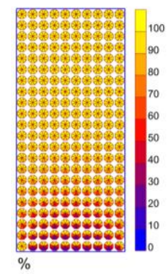
	7	6*10	15˚	95.59	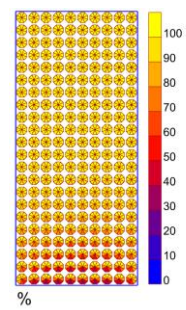
	8	6*10	30˚	95.32	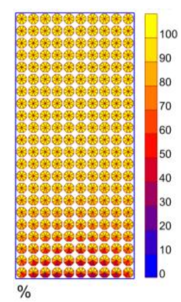
	9	6*10	45˚	94.94	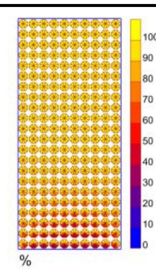

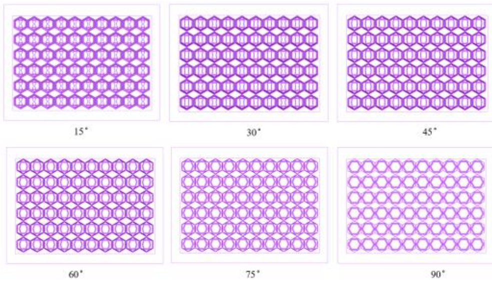	10	6*10	60˚	94.5	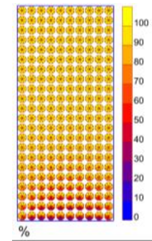
	11	6*10	75˚	94	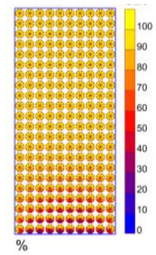
	12	6*10	90˚	93.59	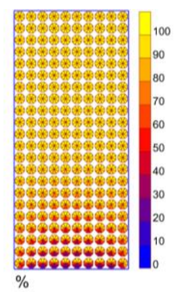

Table 4.12. Glare performance results for each scenario based on % Time DGP < 0.45. Visual comfort is illustrated using color-coded glare maps.
Source: Author's annual glare simulation using Honeybee.

6×10 Panel Configuration (Scenarios 1–12): Both designs within the 6×10 panel group demonstrated strong glare control across all actuator angles. In the first design (Scenarios 1–6), the % Time DGP < 0.45 ranged from 95.49% at 15° to 91.81% at 90°, showing a gradual reduction in visual comfort as actuation increased. This trend suggests that while wider openings allow more daylight, they also allow for slightly more potential glare, though still within acceptable limits.

The second design (Scenarios 7–12) exhibited a similar pattern, with values ranging from 95.59% at 15° to 93.59% at 90°. All values across both designs remained above 90%, indicating effective glare mitigation and confirming that the 6×10 panel configuration maintains a consistently comfortable visual environment, even as geometry transforms dynamically.

<table>
<tr><th>Scenario</th><th>Num</th><th>Number of Auxetic panels (x*y)</th><th>Actuator Degree</th><th>% Time DGP < 0.45</th><th>Visualization</th></tr>
<tr><td rowspan="3">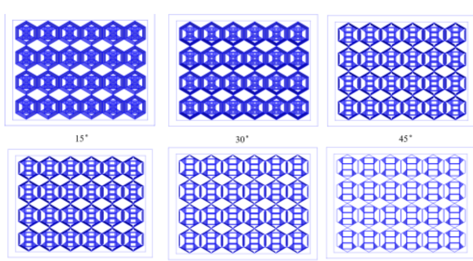</td><td>13</td><td>4*6</td><td>15˚</td><td>96</td><td>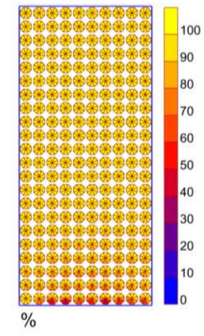</td></tr>
<tr><td>14</td><td>4*6</td><td>30˚</td><td>95.18</td><td>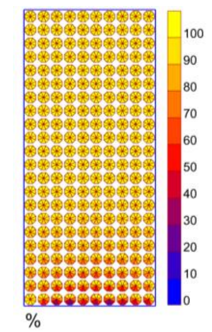</td></tr>
<tr><td>15</td><td>4*6</td><td>45˚</td><td>94.71</td><td>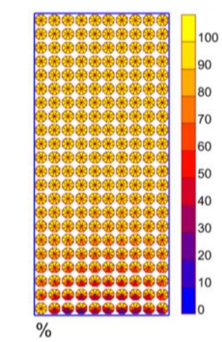</td></tr>
</table>

	16	4*6	60˚	93.15	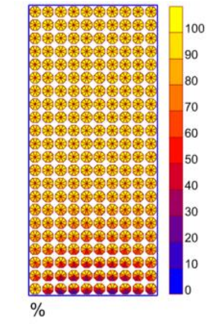
	17	4*6	75˚	92.38	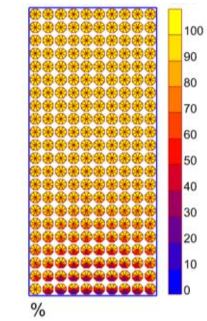
	18	4*6	90˚	91.34	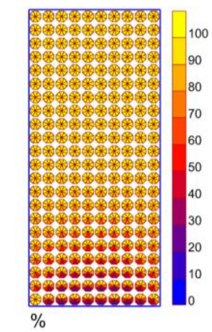
	19	4*6	15˚	96.63	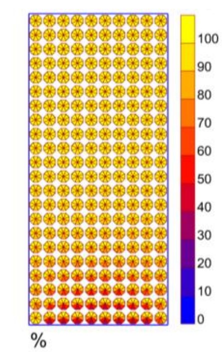

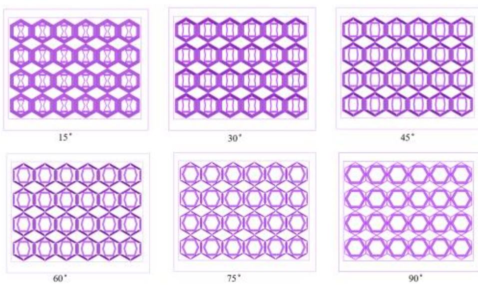	20	4*6	30˚	95.35	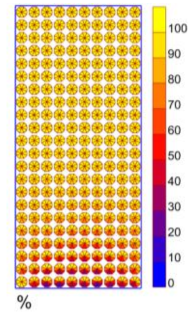
	21	4*6	45˚	95.99	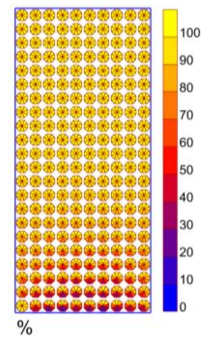
	22	4*6	60˚	94.89	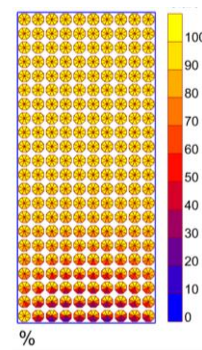
	23	4*6	75˚	94.16	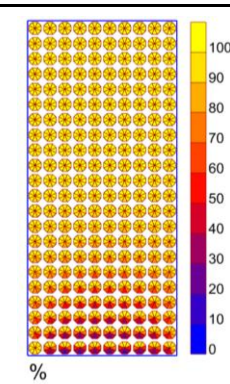

	24	4*6	90˚	93.71	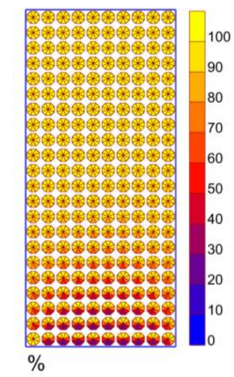

Table 4.13. Glare performance results for the 4×6 auxetic panel configuration based on % Time DGP < 0.45. Visual comfort is illustrated using color-coded glare maps. *Source: Author's annual glare simulation using Honeybee.*

4×6 Panel Configuration (Scenarios 13–24): The 4×6 panel configuration yielded some of the highest DGP comfort scores across the entire dataset. In the first design (Scenarios 13–18), DGP performance peaked at 96% at 15°, gradually reducing to 91.34% at 90°, following a similar downward trend observed in other panel groups. However, the second design (Scenarios 19–24) showed slightly stronger performance overall, with DGP values ranging from 96.63% at 15° to 93.71% at 90°. These consistently high scores across all actuator positions highlight the strength of the 4×6 panel setup in managing glare, particularly in conjunction with its excellent daylight performance. For example, Scenario 24 (4×6, 90°) not only maintained 93.71% visual comfort but also achieved UDI = 79% and sDA = 61.36%, making it a standout in both daylight sufficiency and glare control.

Scenario	Num	Number of Auxetic panels (x*y)	Actuator Degree	% Time DGP < 0.45	Visualization
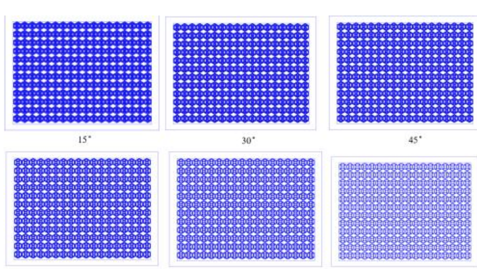	25	12*18	15˚	95.46	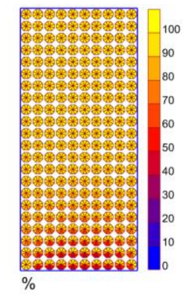
	26	12*18	30˚	95.2	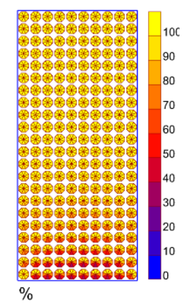
	27	12*18	45˚	94.75	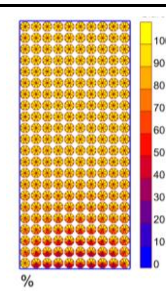
	28	12*18	60˚	94.12	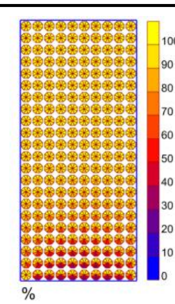

	29	12*18	75°	93.23	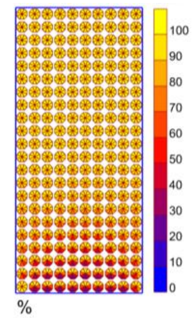
	30	12*18	90°	92	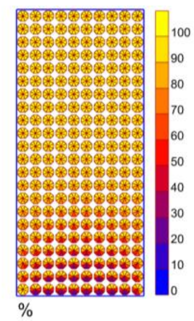
	31	12*18	15°	94.68	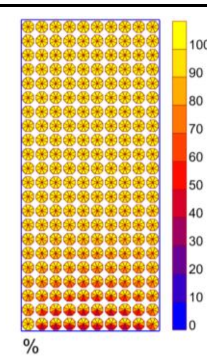
	32	12*18	30°	94.42	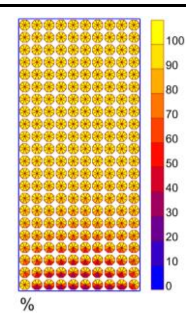

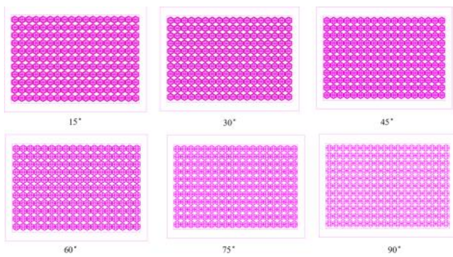	33	12*18	45˚	94	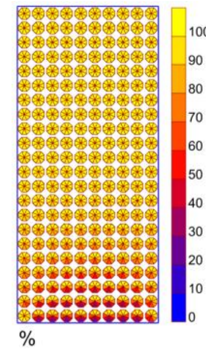
	34	12*18	60˚	93.64	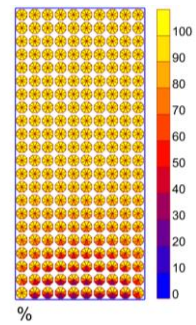
	35	12*18	75˚	93.19	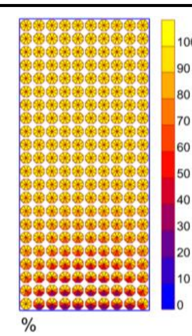
	36	12*18	90˚	93.75	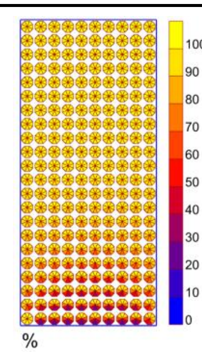

Table 4.14. Glare performance results for the 12×18 auxetic panel configuration based on % Time DGP < 0.45. Visual comfort is represented through color-coded glare maps. *Source: Author's annual glare simulation using Honeybee.*

12×18 Panel Configuration (Scenarios 25–36): The 12×18 high-density panel configuration showed stable and reliable glare control across both designs. The first design (Scenarios 25–30) ranged from 95.46% at 15° to 92% at 90°, showing a consistent and gradual decrease in comfort percentage with increasing actuation.

The second design (Scenarios 31–36) followed a similar trend, starting at 94.68% at 15° and ending at 93.75% at 90°. These results confirm that larger panel densities provide both light diffusion and robust glare resistance, even under highly open conditions. While these scenarios didn't reach the peak daylight performance of some smaller panel configurations, they offered a dependable balance across all visual comfort metrics.

To contextualize these findings, all auxetic configurations were compared against a baseline (non-responsive) façade, which delivered:

Metric Value	Value (%)
UDI	83.22
Sda	77
% Time DGP < 0.45	87.1

Table 4.15. Daylighting and glare performance metrics for the baseline façade configuration with no external shading. This serves as the comparative benchmark for all auxetic scenarios. *Source: Author's simulation outputs using Honeybee.*

These base values represent a highly efficient design condition with no external shading system applied, yet still achieving high daylight sufficiency and strong glare control. This performance demonstrates the effectiveness of the base configuration under clear sky conditions. However, unlike the base case, the auxetic façade scenarios incorporate responsive, geometry-based shading strategies, which offer additional adaptability to changing solar positions. This integration allows the design to maintain visual comfort dynamically and opens new architectural possibilities through material transformation and parametric control.

Among all tested configurations, Scenario 24 (4×6 panel layout, 90° actuator angle) emerged as the most balanced and optimal solution, achieving:

Metric Value	Value (%)
UDI	79
Sda	61.36
% Time DGP < 0.45	93.71

Table 4.16. Performance metrics of the optimal responsive façade scenario (4×6 auxetic panel, 90° actuator angle). This configuration offers the best balance between daylight sufficiency and glare control. *Source: Author's simulation results using Honeybee.*

This comparison illustrates a critical distinction between static, unshaded configurations and adaptive, geometry-driven systems. While the baseline façade performed well under standard conditions—achieving UDI of 83.22%, sDA of 77%, and 87.1% visual comfort time (DGP < 0.45)—its lack of responsiveness to variable sky conditions and solar angles limits its ability to maintain balanced daylight performance throughout the year. The absence of any shading intervention, while beneficial for maximizing daylight availability, inherently risks periods of visual discomfort and overheating during peak sun hours.

In contrast, Scenario 24, featuring a 4×6 auxetic panel array at 90° actuation, demonstrated a highly effective balance between daylight autonomy and glare mitigation. Despite a slightly lower UDI (79%) and sDA (61.36%) compared to the base case, this configuration achieved a notably higher DGP comfort rate of 93.71%, reflecting superior visual comfort performance. This result is significant given the smaller panel density, which implies material efficiency, structural simplicity, and potentially lower cost.

What distinguishes Scenario 24 is its adaptive response: the auxetic geometry actively modulates its aperture in response to solar incidence, controlling daylight penetration and glare simultaneously. This responsiveness enables the system to maintain comfortable interior lighting conditions without relying on mechanical systems or static external shading devices. Moreover, the geometric transformation of the façade presents opportunities for aesthetic variability, bioclimatic integration, and parametric customization for different climates or building orientations.

These results validate the research hypothesis that auxetic structures can be effectively employed in responsive façade design to enhance visual comfort and daylight performance. Furthermore, this study contributes to the evolving discourse on adaptive architecture by offering a novel application of auxetic materials, bridging the gap between material behavior and occupant-centric environmental performance.

5.Conclusion and Recommendations

This research successfully demonstrates how auxetic materials can transform responsive façade design to enhance daylight performance in office buildings. By merging parametric modeling with structural and environmental simulations, the study reveals how auxetic geometries—with their unique negative Poisson's ratio—can passively adapt to sunlight, improving both energy efficiency and occupant comfort.

The investigation tested 36 distinct panel configurations through a rigorous workflow combining Rhino/Grasshopper for geometric design, Karamba3D for structural validation, and Honeybee/Ladybug for daylight analysis. Key findings show that auxetic façades effectively balance daylight provision and glare control. The standout configuration—4×6 panels at 90°

actuation—achieved 79% UDI (daylight usability), 61.36% sDA (spatial daylight coverage), and 93.71% glare comfort, outperforming unshaded designs in visual comfort while maintaining adaptive flexibility.

Structurally, the panels exhibited confirmed auxetic behavior, with Poisson's ratios as low as -1.15, proving their mechanical viability. This material-driven approach eliminates the need for complex mechanical systems, offering a simpler, more sustainable path to dynamic shading.

However, challenges remain in scaling up production and testing real-world performance across diverse climates. Future work should explore physical prototyping, cost-effective fabrication methods, and integration with smart building systems.

By bridging material science and architecture, this research opens new possibilities for adaptive, high-performance building envelopes. The results provide actionable insights for designers seeking innovative solutions that prioritize both sustainability and human-centric environments, marking a step forward in the evolution of responsive architecture.

6.References:

1. Yi, Hwang, and Yuri Kim. 2021. "Prototyping of 4D-Printed Self-Shaping Building Skin in Architecture: Design, Fabrication, and Investigation of a Two-Way Shape Memory Composite (TWSMC) Façade Panel." *Journal of Building Engineering* 43 (February): 103076. https://doi.org/10.1016/j.jobe.2021.103076.

2. Li, Dong, Jie Ma, Liang Dong, and Roderic S. Lakes. 2016. "A Bi-Material Structure with Poisson's Ratio Tunable from Positive to Negative via Temperature Control." *Materials Letters* 181: 285–88. https://doi.org/10.1016/j.matlet.2016.06.054.

3. Zhang, Jianjun, Guoxing Lu, and Zhong You. 2020. "Large Deformation and Energy Absorption of Additively Manufactured Auxetic Materials and Structures: A Review." *Composites Part B: Engineering* 201 (April): 108340. https://doi.org/10.1016/j.compositesb.2020.108340.

4. Gromat, Theo, Julien Gardan, Omar Saifouni, Ali Makke, and Naman Recho. 2023. "Generative Design for Additive Manufacturing of Polymeric Auxetic Materials Produced by Fused Filament Fabrication." *International Journal on Interactive Design and Manufacturing* 17 (6): 2943–55. https://doi.org/10.1007/s12008-022-01102-w.

5. M. B. Ramzan, A. Imran, S. uz Zaman, M. Ali, T. Islam, and A. Rasheed, "Design and development of auxetic structures for enhancing ergonomic comfort in women's intimate apparel (brassiere)," *J. Eng. Fiber. Fabr.*, vol. 18, 2023, doi: 10.1177/15589250231219760.

6. T. Lut, "Application of auxetic materials in modern car industry and future trends," pp. 1–34, 2023.

7. Z. Wang, A. Zulifqar, and H. Hu, "Auxetic composites in aerospace engineering," *Adv. Compos. Mater. Aerosp. Eng.*, pp. 213–240, 2016, doi: 10.1016/b978-0-08-100037-3.00007-9.

8. M. Mir, U. Ansari, and M. Najabat Ali, "Macro-Scale Model Study of a Tunable Drug Dispensation Mechanism for Controlled Drug Delivery in Potential Wound-Healing Applications," *J. Appl. Biomater. Funct. Mater.*, vol. 15, no. 1, pp. 63–69, 2017, doi: 10.5301/jabfm.5000280.

9. O. Duncan *et al.*, "Review of auxetic materials for sports applications: Expanding options in comfort and protection," *Appl. Sci.*, vol. 8, no. 6, 2018, doi: 10.3390/app8060941.

10. C. Yang, H. D. Vora, and Y. B. Chang, “Evaluation of auxetic polymeric structures for use in protective pads,” *ASME Int. Mech. Eng. Congr. Expo. Proc.*, vol. 9, pp. 1–7, 2016, doi: 10.1115/IMECE201667588.

11. M. Sun, X. Hu, L. Tian, X. Yang, and L. Min, “Auxetic Biomedical Metamaterials for Orthopedic Surgery Applications: A Comprehensive Review,” *Orthop. Surg.*, no. 37, pp. 1801–1815, 2024, doi: 10.1111/os.14142.

12. E. B. Park, Y. C. Jeong, and K. Kang, “A novel auxetic sandwich panel for use in structural applications: Fabrication and parametric study,” *Mater. Today Commun.*, vol. 34, no. January, p. 105383, 2023, doi: 10.1016/j.mtcomm.2023.105383.

13. M. Wallbanks, M. F. Khan, M. Bodaghi, A. Triantaphyllou, and A. Serjouei, “On the design workflow of auxetic metamaterials for structural applications,” *Smart Mater. Struct.*, vol. 31, no. 2, 2022, doi: 10.1088/1361-665X/ac3f78.

14. M. Stavric and A. Wiltsche, “Geometrical Elaboration of Auxetic Structures,” *Nexus Netw. J.*, vol. 21, no. 1, pp. 79–90, 2019, doi: 10.1007/s00004-019-00428-5.

15. J. Zhang, G. Lu, and Z. You, “Large deformation and energy absorption of additively manufactured auxetic materials and structures: A review,” *Compos. Part B Eng.*, vol. 201, no. July, p. 108340, 2020, doi: 10.1016/j.compositesb.2020.108340.

16. T. Li, F. Liu, and L. Wang, “Enhancing indentation and impact resistance in auxetic composite materials,” *Compos. Part B Eng.*, vol. 198, no. May, p. 108229, 2020, doi: 10.1016/j.compositesb.2020.108229.

17. N. Novak, O. Duncan, T. Allen, A. Alderson, M. Vesenjak, and Z. Ren, “Shear modulus of conventional and auxetic open-cell foam,” *Mech. Mater.*, vol. 157, p. 103818, 2021, doi: 10.1016/j.mechmat.2021.103818.

18. X. Huang, Z. Zhang, and J. Wu, “An overview of impact resistance of auxetic lattice structure,” *J. Phys. Conf. Ser.*, vol. 1549, no. 3, 2020, doi: 10.1088/1742-6596/1549/3/032077.

19. M. H. Yoon and J. H. Oh, “Design of multi-auxetic microstructures for sound absorbing applications,” *Adv. Compos. Mater.*, vol. 32, no. 2, pp. 225–236, 2023, doi: 10.1080/09243046.2022.2080992.

20. Y. Han, Y. Zhou, G. Qin, J. Dong, D. S. Galvao, and M. Hu, “Unprecedented mechanical response of the lattice thermal conductivity of auxetic carbon crystals,” *Carbon N. Y.*, vol. 122, pp. 374–380, 2017, doi: 10.1016/j.carbon.2017.06.100.

21. L. Gu, Q. Xu, D. Zheng, H. Zou, Z. Liu, and Z. Du, “Analysis of the mechanical properties of double arrowhead auxetic metamaterials under tension,” *Text. Res. J.*, vol. 90, no. 21–22, pp. 2411–2427, 2020, doi: 10.1177/0040517520924850.

22. J. Liu *et al.*, “A flexible porous chiral auxetic tracheal stent with ciliated epithelium,” *Acta Biomater.*, vol. 124, pp. 153–165, 2021, doi: 10.1016/j.actbio.2021.01.044.

23. Yu, Xianglong, Ji Zhou, Haiyi Liang, Zhengyi Jiang, and Lingling Wu. 2018. “Mechanical Metamaterials Associated with Stiffness, Rigidity and Compressibility: A Brief Review.” *Progress in Materials Science* 94: 114–73.

24. D. EL-Mahdy and M. Ali, “Assessing the solar radiation performance of self-shaded 3D-printed clay-based façades,” *Archit. Eng. Des. Manag.*, vol. 20, no. 2, pp. 249–268, 2024, doi: 10.1080/17452007.2023.2285325.

25. K. City, “Potential energy savings with exterior shades in large office buildings and the impact of discomfort glare Sabine Hoffmann , Eleanor S . Lee Environmental Technologies Area,” no. April, 2015.

26. E. Sorooshnia, M. Rashidi, P. Rahnamayiezekavat, F. Rezaei, and B. Samali, “Optimum external shading system for counterbalancing glare probability and daylight illuminance in Sydney’s residential buildings,” *Eng. Constr. Archit. Manag.*, vol. 30, no. 1, pp. 296–320, 2023, doi: 10.1108/ECAM-03-2021-0191.

27. J. Xiong, A. Tzempelikos, P. Karava, and I. Bilionis, “Dynamic balancing between personalized daylight preferences and lighting energy use,” *Build. Simul. Conf. Proc.*, vol. 2, pp. 1216–1223, 2019.

28. UNEP, 2022 Global Status Report for Buildings and Construction: Towards a Zero-Emission, Efficient and Resilient Buildings and Construction Sector, United Nations Environment Programme, 2022. [Online]. Available: www.globalabc.org.

29. S. Li, D. H. W. Li, W. Chen, S. Lou, and E. K. W. Tsang, “Simple mathematical models to link climate-based daylight metrics with daylight factor metrics and daylighting design implications,” *Heliyon*, vol. 9, no. 5, p. e15786, 2023, doi: 10.1016/j.heliyon.2023.e15786

30. E. Sorooshnia, M. Rashidi, P. Rahnamayiezekavat, F. Rezaei, and B. Samali, “Optimum external shading system for counterbalancing glare probability and daylight illuminance in Sydney’s residential buildings,” *Eng. Constr. Archit. Manag.*, vol. 30, no. 1, pp. 296–320, 2023, doi: 10.1108/ECAM-03-2021-0191.

31. T. A. Ningsih, A. Chintianto, C. Pratomo, M. H. Milleza, M. A. Rahman, and I. Chairunnisa, *Hexagonal Responsive Facade Prototype in Responding Sunlight*, vol. Part F1309. Springer Nature Singapore, 2023. doi: 10.1007/978-981-19-8637-6_36.
32. Y. K. Yi, "Building facade multi-objective optimization for daylight and aesthetical perception," *Build. Environ.*, vol. 156, no. October 2018, pp. 178–190, 2019, doi: 10.1016/j.buildenv.2019.04.002.
33. M. S. Roudsari and M. Pak, "Ladybug: A parametric environmental plugin for grasshopper to help designers create an environmentally-conscious design," *Proc. BS 2013 13th Conf. Int. Build. Perform. Simul. Assoc.*, no. December, pp. 3128–3135, 2013, doi: 10.26868/25222708.2013.2499.
34. Yi, Yun Kyu, Jie Yin, and Yichao Tang. 2018. "Developing an Advanced Daylight Model for Building Energy Tool to Simulate Dynamic Shading Device." *Solar Energy* 163 (July 2017): 140–49. https://doi.org/10.1016/j.solener.2018.01.082.
35. Stavric, Milena, and Albert Wiltsche. 2019. "Geometrical Elaboration of Auxetic Structures." *Nexus Network Journal* 21 (1): 79–90. https://doi.org/10.1007/s00004-019-00428-5.
36. X. Ren, R. Das, P. Tran, T. D. Ngo, and Y. M. Xie, "Auxetic metamaterials and structures: A review," *Smart Mater. Struct.*, vol. 27, no. 2, 2018, doi: 10.1088/1361-665X/aaa61c.
37. K. P. Logakannan, V. Ramachandran, J. Rengaswamy, and D. Ruan, "Dynamic Performance of a 3D Re-entrant Structure," *Mech. Mater.*, vol. 148, no. June, p. 103503, 2020, doi: 10.1016/j.mechmat.2020.103503.
38. N. K. Choudhry, B. Panda, and U. S. Dixit, "Energy Absorption Characteristics of Fused Deposition Modeling 3D Printed Auxetic Re-entrant Structures: A Review," *J. Mater. Eng. Perform.*, vol. 32, no. 20, pp. 8981–8999, 2023, doi: 10.1007/s11665-023-08243-3.
39. Y. Deng, Y. Jin, H. Li, and X. Wang, "A new hybrid auxetic structure capable of uniform deformation exhibits excellent energy absorption," *Smart Mater. Struct.*, 2024, doi: 10.1088/1361-665x/ad62ca.
40. P. Fan, Y. Chen, J. Xiong, and H. Hu, "In-plane mechanical properties of a novel hybrid auxetic structure," *Smart Mater. Struct.*, vol. 31, no. 7, 2022, doi: 10.1088/1361-665X/ac68b5.
41. M. Ramírez *et al.*, "Enhancement of Young's moduli and auxetic windows in laminates with isotropic constituents," *Int. J. Eng. Sci.*, vol. 58, pp. 95–114, 2012, doi: 10.1016/j.ijengsci.2012.03.029.
42. A. Tricarico, W. Lin, and Y. Wang, "High Buckling Strength of Auxetic Carbon Fiber Composite Laminates," *Proceedings of the American Society for Composites*, 2023. Available: https://api.semanticscholar.org/CorpusID:265245146
43. N. TRIPATHI, "A Review on Auxetic Polymeric Materials: Synthetic Methodology, Characterization and their Applications," *J. Polym. Mater.*, vol. 40, no. 3–4, pp. 227–269, 2024, doi: 10.32381/jpm.2023.40.3-4.8.

44. Bera, M., "Auxetic textiles," in *Functional and Technical Textiles*, S. Maity, K. Singha, and P. Pandit, Eds., The Textile Institute Book Series, Woodhead Publishing, 2023, pp. 543-614. doi: 10.1016/B978-0-323-91593-9.00001-8.
45. T. Li, F. Liu, and L. Wang, “Enhancing indentation and impact resistance in auxetic composite materials,” *Compos. Part B Eng.*, vol. 198, no. July, p. 108229, 2020, doi: 10.1016/j.compositesb.2020.108229.
46. Z. Li, K. F. Wang, and B. L. Wang, “Indentation resistance of brittle auxetic structures: Combining discrete representation and continuum model,” *Eng. Fract. Mech.*, vol. 252, no. April, 2021, doi: 10.1016/j.engfracmech.2021.107824.
47. M. Chen, S. Fang, G. Wang, Y. Xuan, D. Gao, and M. Zhang, “Compressive and flexural behaviour of engineered cementitious composites based auxetic structures: An experimental and numerical study,” *J. Build. Eng.*, vol. 86, no. January, p. 108999, 2024, doi: 10.1016/j.jobe.2024.108999.
48. S. Teraiya and S. Kumar, “An investigation on flexural properties of anti-tetrachiral auxetic structures fabricated by material extrusion,” *Mater. Today Proc.*, no. xxxx, 2023, doi: 10.1016/j.matpr.2023.04.228.
49. X. Zhao, L. Wei, D. Wen, G. Zhu, Q. Yu, and Z. D. Ma, “Bending response and energy absorption of sandwich beams with novel auxetic honeycomb core,” *Eng. Struct.*, vol. 247, no. August, 2021, doi: 10.1016/j.engstruct.2021.113204.
50. A. Sorrentino, D. Castagnetti, L. Mizzi, and A. Spaggiari, “Rotating squares auxetic metamaterials with improved strain tolerance,” *Smart Mater. Struct.*, vol. 30, no. 3, 2021, doi: 10.1088/1361-665X/abde50.
51. J. Rasburn, P. G. Mullarkey, K. E. Evans, A. Alderson, S. Ameer-Beg, and W. Perrie, “Auxetic structures for variable permeability systems,” *AIChE J.*, vol. 47, no. 11, pp. 2623–2626, 2001, doi: 10.1002/aic.690471125.
52. N. Grimmelsmann, H. Meissner, and A. Ehrmann, “3D printed auxetic forms on knitted fabrics for adjustable permeability and mechanical properties,” *IOP Conf. Ser. Mater. Sci. Eng.*, vol. 137, no. 1, 2016, doi: 10.1088/1757-899X/137/1/012011.
53. L. Ma *et al.*, “Modal characteristics and damping enhancement of carbon fiber composite auxetic double-arrow corrugated sandwich panels,” *Compos. Struct.*, vol. 203, no. July, pp. 539–550, 2018, doi: 10.1016/j.compstruct.2018.07.006.
54. Y. Wang *et al.*, “Sound absorption performance based on auxetic microstructure model: A parametric study,” *Mater. Des.*, vol. 232, p. 112130, 2023, doi: 10.1016/j.matdes.2023.112130.
55. J. S. Raminhos, J. P. Borges, and A. Velhinho, “Development of polymeric anepectic meshes: Auxetic metamaterials with negative thermal expansion,” *Smart Mater. Struct.*, vol. 28, no. 4, 2019, doi: 10.1088/1361-665X/ab034b.
56. Y. Sakai and M. Ohsaki, “Optimization method for shape design of Auxetic Bending-Active Gridshells using discrete differential geometry,” *Structures*, vol. 34, no. February, pp. 1589–1602, 2021, doi: 10.1016/j.istruc.2021.08.067.

57. N. Easey *et al.*, “Dome-shape auxetic cellular metamaterials: Manufacturing, modeling, and testing,” *Front. Mater.*, vol. 6, no. April, pp. 1–13, 2019, doi: 10.3389/fmats.2019.00086.
58. O. Skarsetz, V. Slesarenko, and A. Walther, “Programmable Auxeticity in Hydrogel Metamaterials via Shape-Morphing Unit Cells,” *Adv. Sci.*, vol. 9, no. 23, pp. 1–8, 2022, doi: 10.1002/advs.202201867.
59. M. K. Luković, “Computational Design of Auxetic Shells,” no. September, 2019, [Online]. Available: www.architecturalgeometry.org/aag18%0Ahttps://lgg.epfl.ch/publications/2019/Mina_Thesis/thesis.pdf
60. X. Xin, L. Liu, Y. Liu, and J. Leng, “4D Printing Auxetic Metamaterials with Tunable, Programmable, and Reconfigurable Mechanical Properties,” *Adv. Funct. Mater.*, vol. 30, no. 43, pp. 1–10, 2020, doi: 10.1002/adfm.202004226.
61. V. A. Lvov, F. S. Senatov, A. A. Veveris, V. A. Skrybykina, and A. Díaz Lantada, “Auxetic metamaterials for biomedical devices: Current situation, main challenges, and research trends,” *Materials*, vol. 15, no. 4, p. 1439, 2022. doi: 10.3390/ma15041439.
62. Shepherd T., H. Driscoll, K. Winwood, Venkatraman, A. Alderson, and T. Allen, “Review of Modelling and Additive Manufacturing of Auxetic Materials for Application in Sport, 8th Asia-Pacific Congress on Sports Technology,” *8th Asia-Pacific Congr. Sport. Technol. (APCST 2017)*, no. October, 2017, [Online]. Available: http://apcstcon.com/
63. M. Razbin, R. Bagherzadeh, M. Asadnia, and S. Wu, “Recent Advances in Wearable Electromechanical Sensors Based on Auxetic Textiles,” *Adv. Funct. Mater.*, vol. 2409242, pp. 1–20, 2024, doi: 10.1002/adfm.202409242.
64. T. Lut, “Application of auxetic materials in modern car industry and future trends,” pp. 1–34, 2023.
65. P. R. Budarapu, Y. B. Sudhir Sastry, and R. Natarajan, “Design concepts of an aircraft wing: composite and morphing airfoil with auxetic structures,” *Front. Struct. Civ. Eng.*, vol. 10, no. 4, pp. 394–408, 2016, doi: 10.1007/s11709-016-0352-z.
66. M. Sadegh Ebrahimi, M. Noruzi, R. Hamzehei, E. Etemadi, and R. Hashemi, “Revolutionary auxetic intravascular medical stents for angioplasty applications,” *Mater. Des.*, vol. 235, no. July, p. 112393, 2023, doi: 10.1016/j.matdes.2023.112393.
67. Y. Jiang *et al.*, “3D-printed auxetic-structured intervertebral disc implant for potential treatment of lumbar herniated disc,” *Bioact. Mater.*, vol. 20, no. October 2021, pp. 528–538, 2023, doi: 10.1016/j.bioactmat.2022.06.002.
68. F. Tsegay, M. Hisham, M. Elsherif, A. Schiffer, and H. Butt, “3D Printing of pH Indicator Auxetic Hydrogel Skin Wound Dressing,” *Molecules*, vol. 28, no. 3, pp. 1–18, 2023, doi: 10.3390/molecules28031339.
69. Y. W. Chen *et al.*, “High-yield extracellular vesicle production from HEK293T cells encapsulated in 3D auxetic scaffolds with cyclic mechanical stimulation for effective

drug carrier systems," *Biofabrication*, vol. 16, no. 4, 2024, doi: 10.1088/1758-5090/ad728b.

70. M. Razbin, R. Bagherzadeh, M. Asadnia, and S. Wu, "Recent Advances in Wearable Electromechanical Sensors Based on Auxetic Textiles," *Adv. Funct. Mater.*, vol. 2409242, pp. 1–20, 2024, doi: 10.1002/adfm.202409242.
71. J. Wienold and J. Christoffersen, "Evaluation methods and development of a new glare prediction model for daylight environments with the use of CCD cameras," *Energy and Buildings*, vol. 38, no. 7, pp. 743–757, 2006. doi: 10.1016/j.enbuild.2006.03.017